was negatively affected if the amount of injected pCMV-Luc exceeded 50 μg/mouse (Figure 4A). This could in part account for the apparent inhibition of transgene expression demonstrated in the report by Budker *et al.* [25], where co-injection of an excess of nonexpressing DNA (500 μg) led to a decrease in reporter gene (pCI-Luc, 50 μg) expression. A prior large-volume injection allowed significant transgene expression by a subsequent naked pDNA injection (Figure 5). The sequential injections at various time intervals revealed that, based on the transgene expression by pCMV-Luc, the effect of the hydrodynamics-based procedure appeared to last more than 15 min and the transient increase in membrane permeability recovered within 30 min.

A significant level of transgene expression was observed in the hepatocyte culture isolated immediately after gene delivery (Figure 6), suggesting that pDNA might be delivered intracellularly with a potential for successful transgene expression following the hydrodynamics-based procedure within the period during which the cell membrane was affected and rendered permeable. However, we cannot yet exclude the possibility that 10 min as perfusion period is sufficient for completion of receptor-mediated internalization of pDNA and that DNA molecules located outside of the cells at the time of isolation would enter the cells afterwards and lead to transgene expression. Hydrodynamics-based injection of luciferase-expressing RNA, which is supposed to proceed translation once delivered intracellularly, resulted in a significant level of transgene expression as early as 10 min after injection (Figure 7). This indicates that intracellular delivery of some RNA has been completed immediately after injection, although a specified period of time appears necessary for completion of mRNA translation. Taken together, although DNA and RNA possess different characteristics such as chemical structure and stability, these results suggest that pDNA might be delivered intracellularly within a short period with a transgene expression potential following the hydrodynamics-based procedure. Therefore, a large portion of the pDNA bound to the outside surface of the plasma membrane for a relatively long time [25,32] might not make a significant contribution to transgene expression. Instead, such pDNA is likely to undergo degradation by accessible external DNase or lysosomal degradation followed by internalization.

We studied the plasma concentration profiles of ALT and AST following the hydrodynamics-based procedure, especially focusing on the earliest phase after injection. As expected from the notion of increased membrane permeability, the highest levels of plasma ALT and AST were observed at 10 min and 4 h (Figure 3). An actual amount of those enzymes detected at 10 min could be higher than that at 4 h, because the blood should be diluted to some extent by the large volume of injected solution immediately after injection. This indicates that the hepatic enzymes ALT and AST immediately diffused out of the hepatocytes following the hydrodynamics-based procedure and were then eliminated gradually from the circulation depending on their pharmacokinetic characteristics, although there should be a possibility that all the observed ALT and AST was simply due to cell death or severe damages caused on some of the hepatocytes that were different from those expressing the transgene. Since ALT and AST are well-known indicators of liver damage, one might think that the values observed in the present study indicate that this procedure is toxic. However, based on the facts that the increased permeability of the cell membrane is only transient and recovered within 30 min, leakage of those enzymes is not totally due to cellular apoptosis or necrosis, but is a transient event caused by the injection procedure. In other words, to accomplish an efficient intracellular delivery of pDNA, an extremely large molecule compared with ALT and AST, it is essential that the hepatocyte cellular membrane is rendered permeable enough to allow transient massive effusion of the hepatic enzymes. The same could apply to the case of gene delivery via electroporation, where the electric pulses open up pores in the cell membranes through which DNA may pass into the interior [34]. From these standpoints, it is conceivable that cellular enzymes such as ALT and AST are not appropriate for the safety evaluation of physical gene delivery strategies including the hydrodynamics-based procedure.

Various nonviral delivery systems have been developed with little success in clinical applications. The delivery system internalized successfully by endocytosis confronts the barrier posed by the endosomal trafficking process which, if not escaped, leads to degradation in lysosomes. This barrier causes a massive drop in the population of therapeutic pDNA molecules, which face up to the following barriers of cytosolic metabolism [35] and nuclear membrane [36,37], diminishing markedly the efficiency of conventional delivery systems. However, it is suggested that the hydrodynamics-based procedure allows direct cytosolic delivery of pDNA through the cell membrane. Thus, pDNA can circumvent the endosomal or lysosomal barriers by this procedure, offering the possibility of a pDNA or pDNA/functional carrier complex aimed at nuclear localization.

In conclusion, we have investigated the possible mechanisms for efficient gene transfer by the hydrodynamics-based procedure and suggested that it would involve in part direct cytosolic delivery of pDNA via an influx along with the large volume of injected solution or a diffusion of pDNA through the cell membrane resulting in transiently increased permeability. In spite of recent advances in vector design, progress in nonviral gene therapy has been unexpectedly delayed mainly because of the inefficiency in delivering genes of interest. Although more studies of safety aspects are required, the marked therapeutic benefit compared with the potential risk of the invasive strategy should encourage the application of the hydrodynamics-based procedure with some modifications and/or the use of suitable devices to become a standard methodology for nonviral gene therapy in the immediate future.

Acknowledgement

This work was supported in part by a Grant-in-Aid for Scientific Research from the Ministry of Education, Culture, Sports, Science and Technology, Japan.

References

1. Nishikawa M, Huang L. Nonviral vectors in the new millennium: delivery barriers in gene transfer. *Hum Gene Ther* 2001; **12**: 861–870.
2. Niidome T, Huang L. Gene therapy progress and prospects: nonviral vectors. *Gene Ther* 2002; **9**: 1647–1652.
3. Liu F, Song Y, Liu D. Hydrodynamics-based transfection in animals by systemic administration of plasmid DNA. *Gene Ther* 1999; **6**: 1258–1266.
4. Zhang G, Budker V, Wolff JA. High levels of foreign gene expression in hepatocytes after tail vein injections of naked plasmid DNA. *Hum Gene Ther* 1999; **10**: 1735–1737.
5. Song YK, Liu F, Zhang G, *et al.* Hydrodynamics-based transfection: simple and efficient method for introducing and expressing transgenes in animals by intravenous injection of DNA. *Methods Enzymol* 2002; **346**: 92–105.
6. Kobayashi N, Kuramoto T, Chen S, *et al.* Therapeutic effect of intravenous interferon gene delivery with naked plasmid DNA in murine metastasis models. *Mol Ther* 2002; **6**: 737–744.
7. Kobayashi N, Matsui Y, Kawase A, *et al.* Vector-based in vivo RNA interference: dose- and time-dependent suppression of transgene expression. *J Pharmacol Exp Ther* 2004; **308**: 688–693.
8. Kobayashi N, Hirata K, Chen S, *et al.* Hepatic delivery of particulates in the submicron range by a hydrodynamics-based procedure: implications for particulate gene delivery systems. *J Gene Med* 2004; in press.
9. Wu X, He Y, Falo LD Jr, *et al.* Regression of human mammary adenocarcinoma by systemic administration of a recombinant gene encoding the hFlex-TRAIL fusion protein. *Mol Ther* 2001; **3**: 368–374.
10. Wang Z, Qiu SJ, Ye SL, *et al.* Combined IL-12 and GM-CSF gene therapy for murine hepatocellular carcinoma. *Cancer Gene Ther* 2001; **8**: 751–758.
11. Chang J, Sigal LJ, Lerro A, *et al.* Replication of the human hepatitis delta virus genome is initiated in mouse hepatocytes following intravenous injection of naked DNA or RNA sequences. *J Virol* 2001; **75**: 3469–3473.
12. He Y, Pimenov AA, Nayak JV, *et al.* Intravenous injection of naked DNA encoding secreted flt3 ligand dramatically increases the number of dendritic cells and natural killer cells in vivo. *Hum Gene Ther* 2000; **11**: 547–554.
13. Zhang G, Song YK, Liu D. Long-term expression of human alpha1-antitrypsin gene in mouse liver achieved by intravenous administration of plasmid DNA using a hydrodynamics-based procedure. *Gene Ther* 2000; **7**: 1344–1349.
14. Maruyama H, Higuchi N, Nishikawa Y, *et al.* High-level expression of naked DNA delivered to rat liver via tail vein injection. *J Gene Med* 2002; **4**: 333–341.
15. Yang J, Chen S, Huang L, *et al.* Sustained expression of naked plasmid DNA encoding hepatocyte growth factor in mice promotes liver and overall body growth. *Hepatology* 2001; **33**: 848–859.
16. Miao CH, Thompson AR, Loeb K, *et al.* Long-term and therapeutic-level hepatic gene expression of human factor IX after naked plasmid transfer in vivo. *Mol Ther* 2001; **3**: 947–957.
17. Yang J, Dai C, Liu Y. Systemic administration of naked plasmid encoding hepatocyte growth factor ameliorates chronic renal fibrosis in mice. *Gene Ther* 2001; **8**: 1470–1479.
18. Budker V, Zhang G, Knechtle S, *et al.* Naked DNA delivered intraportally expresses efficiently in hepatocytes. *Gene Ther* 1996; **3**: 593–598.
19. Zhang G, Vargo D, Budker V, *et al.* Expression of naked plasmid DNA injected into the afferent and efferent vessels of rodent and dog livers. *Hum Gene Ther* 1997; **8**: 1763–1772.
20. Zhang G, Budker V, Williams P, *et al.* Efficient expression of naked DNA delivered intraarterially to limb muscles of nonhuman primates. *Hum Gene Ther* 2001; **12**: 427–438.
21. Budker V, Zhang G, Danko I, *et al.* The efficient expression of intravascularly delivered DNA in rat muscle. *Gene Ther* 1998; **5**: 272–276.
22. Maruyama H, Higuchi N, Nishikawa Y, *et al.* Kidney-targeted naked DNA transfer by retrograde renal vein injection in rats. *Hum Gene Ther* 2002; **13**: 455–468.
23. Zhang G, Budker V, Williams P, *et al.* Surgical procedures for intravascular delivery of plasmid DNA to organs. *Methods Enzymol* 2002; **346**: 125–133.
24. Eastman SJ, Baskin KM, Hodges BL, *et al.* Development of catheter-based procedures for transducing the isolated rabbit liver with plasmid DNA. *Hum Gene Ther* 2002; **13**: 2065–2077.
25. Budker V, Budker T, Zhang G, *et al.* Hypothesis: naked plasmid DNA is taken up by cells in vivo by a receptor-mediated process. *J Gene Med* 2000; **2**: 76–88.
26. Kobayashi N, Kuramoto T, Yamaoka K, *et al.* Hepatic uptake and gene expression mechanisms following intravenous administration of plasmid DNA by conventional and hydrodynamics-based procedures. *J Pharmacol Exp Ther* 2001; **297**: 853–860.
27. Aronheim A, Engelberg D, Li N, *et al.* Membrane targeting of the nucleotide exchange factor Sos is sufficient for activating the Ras signaling pathway. *Cell* 1994; **78**: 949–961.
28. Hancock JF, Cadwallader K, Marshall CJ. Methylation and proteolysis are essential for efficient membrane binding of prenylated p21K-ras(B). *EMBO J* 1991; **10**: 641–646.
29. Nomura T, Yasuda K, Yamada T, *et al.* Gene expression and antitumor effects following direct interferon (IFN)-gamma gene transfer with naked plasmid DNA and DC-chol liposome complexes in mice. *Gene Ther* 1999; **6**: 121–129.
30. Nishikawa M, Takemura S, Takakura Y, *et al.* Targeted delivery of plasmid DNA to hepatocytes in vivo: optimization of the pharmacokinetics of plasmid DNA/galactosylated poly(L-lysine) complexes by controlling their physicochemical properties. *J Pharmacol Exp Ther* 1998; **287**: 408–415.
31. Rossmanith W, Chabicovsky M, Herkner K, *et al.* Cellular gene dose and kinetics of gene expression in mouse livers transfected by high-volume tail-vein injection of naked DNA. *DNA Cell Biol* 2002; **21**: 847–853.
32. Lecocq M, Andrianaivo F, Warnier MT, *et al.* Uptake by mouse liver and intracellular fate of plasmid DNA after a rapid tail vein injection of a small or a large volume. *J Gene Med* 2003; **5**: 142–156.
33. Herweijer H, Zhang G, Subbotin VM, *et al.* Time course of gene expression after plasmid DNA gene transfer to the liver. *J Gene Med* 2001; **3**: 280–291.
34. Somiari S, Glasspool-Malone J, Drabick JJ, *et al.* Theory and in vivo application of electroporative gene delivery. *Mol Ther* 2000; **2**: 178–187.
35. Lechardeur D, Sohn KJ, Haardt M, *et al.* Metabolic instability of plasmid DNA in the cytosol: a potential barrier to gene transfer. *Gene Ther* 1999; **6**: 482–497.
36. Wilke M, Fortunati E, van den Broek M, *et al.* Efficacy of a peptide-based gene delivery system depends on mitotic activity. *Gene Ther* 1996; **3**: 1133–1142.
37. Zabner J, Fasbender AJ, Moninger T, *et al.* Cellular and molecular barriers to gene transfer by a cationic lipid. *J Biol Chem* 1995; **270**: 18 997–19 007.

THE JOURNAL OF GENE MEDICINE
J Gene Med 2004; 6: 455–463.
Published online 16 February 2004 in Wiley InterScience (www.interscience.wiley.com). DOI: 10.1002/jgm.531

RESEARCH ARTICLE

Hepatic delivery of particulates in the submicron range by a hydrodynamics-based procedure: implications for particulate gene delivery systems

Naoki Kobayashi
Kazuhiro Hirata
Shi Chen
Atsushi Kawase
Makiya Nishikawa
Yoshinobu Takakura*

Department of Biopharmaceutics and Drug Metabolism, Graduate School of Pharmaceutical Sciences, Kyoto University, Sakyo-ku, Kyoto 606-8501, Japan

*Correspondence to:
Yoshinobu Takakura, Department of Biopharmaceutics and Drug Metabolism, Graduate School of Pharmaceutical Sciences, Kyoto University, Sakyo-ku, Kyoto 606-8501, Japan.
E-mail:
takakura@pharm.kyoto-u.ac.jp

Received: 15 July 2003
Revised: 17 November 2003
Accepted: 20 November 2003

Abstract

Background A large-volume intravenous (i.v.) injection of DNA, i.e. a hydrodynamics-based transfection procedure, is known to be an efficient and liver-specific method of *in vivo* gene delivery. However, little is available on an applicable particle size in the procedure.

Methods We examined the effect of particle size on the hepatic delivery by the hydrodynamics-based procedure, using fluorescein isothiocyanate labeled polystyrene microspheres (MS) of 50, 200 or 500 nm in diameter. MS were injected intravenously to mice by a conventional (normal) or the hydrodynamics-based procedure and their degree of hepatic uptake was determined fluorometrically.

Results For all sizes tested, the two procedures were similar in terms of the apparent degree of hepatic uptake, whereas the intrahepatic localization of MS was apparently different between the procedures as shown by an examination of frozen tissue sections. In mice with gadolinium chloride induced Kupffer cell blockade, the hepatic uptake of MS following the normal procedure was decreased while that of the hydrodynamics-based procedure was less affected. This phenomenon of enhanced hepatic delivery seemed to be more effective for larger particles. Confocal microscopic observation of hepatocyte suspensions indicated that part of the injected MS-50 was delivered intracellularly following the hydrodynamics-based procedure, whereas almost all the observed MS-200 and MS-500 were detected in the extracellular compartment or on the surface of the cells. This was supported by the fact that most of the injected MS existed pericellularly around the transgene-expressing cells.

Conclusions The hydrodynamics-based procedure facilitated extravasation and hepatic delivery of MS. Larger MS were more efficiently extravasated and trapped by the liver, whereas intracellular delivery hardly occurred with them. Copyright © 2004 John Wiley & Sons, Ltd.

Keywords hydrodynamics-based procedure; microsphere; liver; particle size; plasmid DNA; hepatocyte

Introduction

A high-speed intravenous (i.v.) administration of a large volume of solution containing naked plasmid DNA (pDNA), the so-called hydrodynamics-based procedure, resulted in an astonishingly high level of transgene expression in the liver of mice [1,2]. This procedure has

been gaining attention due to its potential as an alternative gene delivery technique for therapeutic purposes in addition to its usefulness as a convenient *in vivo* transfection method for laboratory animals [3,4]. While we and other groups have clarified the fate of the injected pDNA and the transgene expression profiles following this procedure [5–10], the mechanism behind the efficient hepatic uptake of pDNA, which leads to a significant transgene expression, is still controversial and remains to be elucidated. In our previous study, it was found that macromolecules such as bovine serum albumin and immunoglobulin G, but not polyethylene glycol with a molecular weight of 4000, were efficiently taken up by the liver following a large-volume injection [5], suggesting that the hydrodynamics-based procedure caused hepatic delivery of diverse macromolecules of relatively large molecular weight. However, as well as the lack of clarity about the hepatic uptake mechanism, there is also a lack of information about the effects of the solute size on the efficacy of the procedure.

The principle of the hydrodynamics-based procedure could be applicable to an organ-restricted gene delivery method; e.g. targeting the liver by injection via the portal vein with transient occlusion of the outflow as demonstrated earlier [11,12] and by the catheter-mediated hydrodynamics-based delivery reported very recently [13]. This method allows conventional naked pDNA to be effective enough to obtain therapeutic levels of target transgene products [6,14–16]. Actually, complexation of pDNA with some cationic molecules such as liposomes or polymer impeded the efficacy of transgene expression following the hydrodynamics-based procedure, indicating that the 'nakedness' of the injected pDNA was an important factor [9, Kobayashi *et al.*, unpublished observation]. However, lack of long-term transgene expression probably due to rapid promoter inactivation [7,17] would require repeated administration. This underlines the importance of strategies such as complexation or encapsulation of pDNA, in addition to improvement in the pDNA backbone such as via Epstein-Barr virus-based plasmid vector [18] or CpG-depleted vector [19]. These complexation or encapsulation strategies include some promising carriers; e.g. polyethylenimine for increasing nuclear localization [20] or biodegradable polymer for controlled release of therapeutic pDNA [21]. One of the problems associated with these particle-based gene delivery systems is the lack of information about whether hydrodynamics-based transfection could effectively work on such particle sizes. Since the hydrodynamics-based procedure is likely to result in direct intracellular delivery of pDNA via cellular membrane [5,22], its delivery efficiency would be largely influenced by the particle size although other factors such as net surface charge might also have some effects. To develop optimal strategies for a particle-based gene delivery, it is essential to clarify the particle size dependence of the hydrodynamics-based procedure.

In the present study, therefore, we examined the effect of particle size on the enhanced hepatic delivery via the hydrodynamics-based procedure. Fluorescein isothiocyanate labeled polystyrene microspheres (MS) were used as model particles due to their narrow size dispersion and their biological stability so that we could examine precisely the effect of particle size. MS of 50, 200 and 500 nm in size were employed for the present study, assuming that the size of pDNA/functional carrier complexes reported to date was in the 100-nanometer range. The effects of particle size on the apparent degree of hepatic uptake of MS were studied quantitatively by comparing two i.v. injection procedures: the normal and the hydrodynamics-based procedure. Intrahepatic distribution of MS was also discussed in relation to the particle size. We found that larger MS were more efficiently extravasated and trapped by the liver, whereas intracellular delivery hardly occurred at all if the particle size exceeded putatively 50 nm.

Materials and methods

Chemicals

Monodispersed and non-ionized polystyrene microspheres (MS), covalently linked with fluorescein isothiocyanate (FITC), 50, 200 and 500 nm in diameter (MS-50, MS-200 and MS-500, respectively), were purchased from Polysciences, Inc. (Warrington, PA, USA) and used for all experiments in the present study. Gadolinium chloride ($GdCl_3$) was purchased from Sigma (St. Louis, MO, USA). Red fluorescent protein expressing pDNA, pDsRed2-N1, purchased from BD Biosciences Clontech (Palo Alto, CA, USA), was amplified in the DH5α strain of *Escherichia coli* and purified using a QIAGEN Endofree Plasmid Giga kit (QIAGEN GmbH, Hilden, Germany). All other chemicals used were of the highest purity available.

Mice and i.v. injection of MS

Four-week-old female ddY mice (approximately 20 g body weight), purchased from Shizuoka Agricultural Cooperative Association for Laboratory Animals (Shizuoka, Japan), were used for all experiments. Mice received each size of MS (12.5 mg/kg) dissolved in saline (Otsuka, Tokyo, Japan) by tail vein injection. In the cases mentioned, mice received MS (12.5 mg/kg) and *Discosoma* sp. red fluorescent protein (DsRed)-expressing pDNA, pDsRed2-N1 (25 μg/mouse), simultaneously by a single tail vein injection. The volume of injected solution was 100 μl or 1.6 ml for the normal or the hydrodynamics-based procedure, respectively. The tail vein injection was performed over less than 5 s using a 26-gauge needle for both procedures.

Quantitative analysis of MS

The degree of hepatic uptake and the blood concentrations of MS were determined fluorometrically according

to our previous reports [23,24]. The whole liver was excised from mice at the indicated time, homogenized with an equal volume (v/w) of distilled water, and subjected to three cycles of freezing (−190 °C) and thawing (37 °C) to destroy the cells completely. Blood was withdrawn from the vena cava and 100 µl were mixed with 5 ml distilled water containing EDTA (0.1 mM) to complete hemolysis. The liver homogenate and the blood samples were lyophilized and then suspended in an accurately measured volume of chloroform and incubated at 30 °C for 18 h with gentle mechanical shaking to extract FITC of MS. Following filtration of the resulting suspension through a 0.45 µm membrane filter (Millipore, Billerica, MA, USA), its fluorescence was measured in a spectrofluorophotometer (RF-540; Shimadzu, Kyoto, Japan) operated at an excitation wavelength of 458 nm and an emission wavelength of 540 nm. As a standard, the liver homogenate or the blood obtained from age-matched untreated mice was combined with a known amount of injected solution and subjected to the same steps.

Confocal microscopic study

At the described intervals following MS injection, mice were sacrificed and the liver was gently infused with 5 ml saline through the portal vein to remove remaining blood. The liver was then embedded in Tissue-Tek OCT embedding compound (Sakura Finetechnical Co., Ltd., Tokyo, Japan), frozen in liquid nitrogen and stored in 2-methylbutanol at −80 °C. Frozen liver sections were made, 8 µm in thickness, using a cryostat (Jung Frigocut 2800E; Leica Microsystems AG, Wetzlar, Germany) by the routine procedure and fixed with Mildform 20N (Wako, Osaka, Japan). For nucleus staining, the section was incubated with 15 µg/ml RNase (type I-A; Sigma) at 37 °C for 20 min followed by 0.5 mg/ml propidium iodide (Sigma) at room temperature for 20 min. The sections were examined by confocal laser scanning microscopy (MRC-1024; BioRad, Hercules, CA, USA). In the case of simultaneous injection of MS and pDsRed2-N1, frozen liver sections were directly subjected to confocal microscopic observation without any fixation, since the fixation step caused massive loss of DsRed protein due to immediate dissolution in the fixation buffer in our preliminary experiments. For cellular suspensions, X-Z scanning and sequential X-Y scanning were performed to distinguish intracellular fluorescent signals from those on the cellular membrane.

$GdCl_3$-induced Kupffer cell blockade

Gadolinium chloride ($GdCl_3$) is supposed to form colloidal particles in the blood and to cause apoptosis of Kupffer cells following i.v. injection [25]. $GdCl_3$ (30 mg/kg) was injected intravenously into mice 24 h before MS injection. This dosage had proved to be enough to induce Kupffer cell blockade in a previous study [5].

Isolation of cellular suspension of hepatocytes

To evaluate the intrahepatic cellular distribution of MS, liver parenchymal cells and nonparenchymal cells were isolated by differential centrifugation according to a previous report [26]. Briefly, mice were sacrificed 10 min after injection of MS (12.5 mg/kg) by the normal or the hydrodynamics-based procedure and the liver was digested with collagenase (type I; Sigma) and fractionated into hepatocytes and nonparenchymal cells by differential centrifugation. The cellular suspension of hepatocytes was adjusted to 1×10^5 cells/ml with Hank's-HEPES buffer, mixed with a nine-fold volume of 100% glycerol to increase the viscosity, and dribbled onto glass slides for subsequent confocal microscopic observation. The hepatocytes were identified based on their larger size under microscopic observation and their purity proved to be always more than 95%.

Results

Comparison of the normal and the hydrodynamics-based procedures for the hepatic uptake of MS

Figure 1 shows the degree of hepatic uptake and the blood concentration of MS following the normal and the hydrodynamics-based procedures. For all sizes tested, the apparent degree of hepatic uptake was similar in both procedures. The absolute values for the degree of hepatic uptake of MS-50 and MS-500 were very similar to those in our previous report involving rats [23,24]. The degree of hepatic uptake was similar in mice sacrificed at 24 h after MS injection (data not shown). The blood concentration of MS following the hydrodynamics-based procedure was lower than that following the normal procedure, probably due to dilution of the blood by the large volume of injected solution. To examine the intrahepatic localization of MS, frozen sections were made following MS injection by the normal and the hydrodynamics-based procedures. As shown in Figure 2, MS accumulated in some specific cells, predominantly Kupffer cells, following the normal procedure (Figures 2A, 2C and 2E), whereas MS appeared to be dispersed more widely following the hydrodynamics-based procedure (Figures 2B, 2D and 2F). It is difficult to discuss the differences between the two procedures quantitatively in terms of the apparent degree of hepatic uptake while the intrahepatic distribution was apparently different.

Comparison of the two procedures for the hepatic uptake of MS in $GdCl_3$-treated mice

To minimize the effect of MS uptake by Kupffer cells, which hampered quantitative comparison of the two

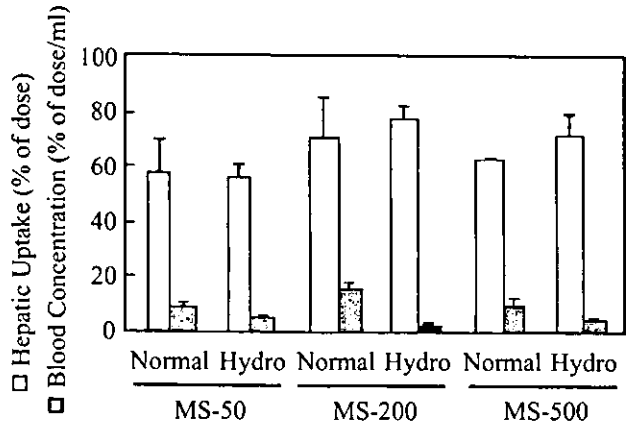

Figure 1. Degree of hepatic uptake and blood concentrations of MS following i.v. injection by the normal and the hydrodynamics-based procedures. Mice received an i.v. injection of MS-50, MS-200 or MS-500 (12.5 mg/kg) by the normal or the hydrodynamics-based procedure and the degree of hepatic uptake and the blood concentrations of MS were determined at 10 min. The results are expressed as the mean ± S.D. of at least three mice. There are no significant differences between the procedures in the degree of hepatic uptake of any size of MS

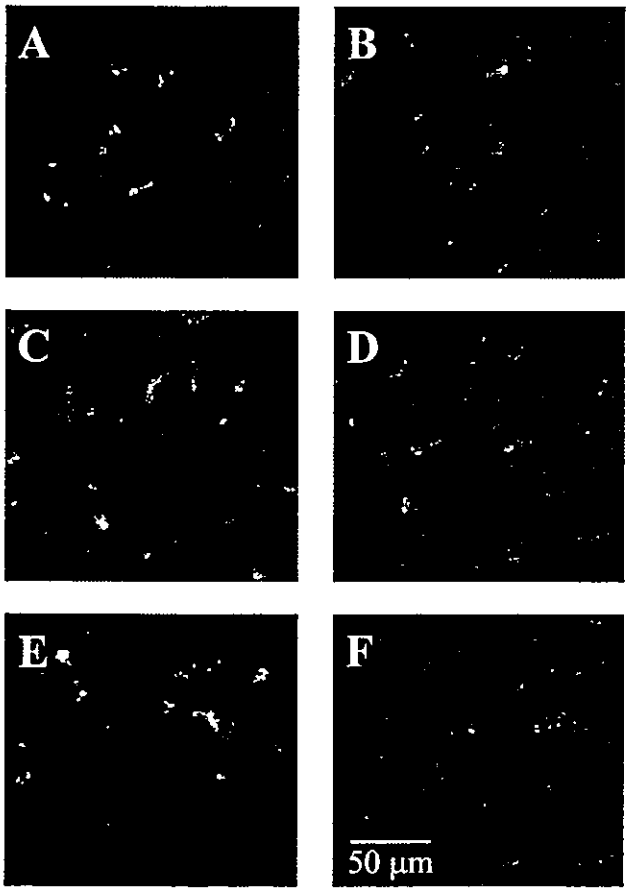

Figure 2. Confocal microscopic images of the liver section following i.v. injections of MS. Liver was excised 10 min after an i.v. injection of MS-50 (A, B), MS-200 (C, D) or MS-500 (E, F) by the normal (A, C, E) or the hydrodynamics-based (B, D, F) procedure. Frozen liver sections were made and stained with propidium iodide. Red: cell nucleus; green: FITC-MS

procedures, $GdCl_3$ was used as a Kupffer cell inhibitor. Figure 3 shows the degree of hepatic uptake and the blood concentration of MS following the normal and the hydrodynamics-based procedures in $GdCl_3$-treated mice. The hepatic uptake of MS and the elimination of MS from the blood were significantly inhibited by $GdCl_3$ treatment as far as the normal procedure was concerned. For all sizes tested, the apparent degree of hepatic uptake following the hydrodynamics-based procedure was significantly higher than that of the normal procedure (Figure 3).

Effect of particle size on the hepatic uptake of MS

To discuss the effect of particle size on the hepatic uptake of MS following the normal and the hydrodynamics-based procedures, the absolute degree of hepatic uptake in the defined control group (i.e. the normal procedure in $GdCl_3$-untreated mice) of MS-50, MS-200 or MS-500 was normalized to 100% and the relative degree of hepatic uptake compared with each corresponding control was calculated. As shown in Table 1, for all sizes tested, the apparent degree of hepatic uptake of MS was dramatically reduced by $GdCl_3$-induced Kupffer cell blockade (Table 1; cf. $GdCl_3(-)$ Normal vs. $GdCl_3(+)$ Normal). Among them, the hepatic uptake of MS-500 was the most susceptible to the Kupffer-cell blockade of $GdCl_3$. However, the apparent degree of hepatic uptake of MS was not affected by $GdCl_3$ for the hydrodynamics-based procedure (Table 1; cf. $GdCl_3(-)$ Hydro vs. $GdCl_3(+)$ Hydro). The larger the particle size, the more dramatically the hepatic uptake of MS was facilitated by the hydrodynamics-based procedure in $GdCl_3$-treated mice (Table 1; cf. $GdCl_3(+)$ Normal vs. $GdCl_3(+)$ Hydro).

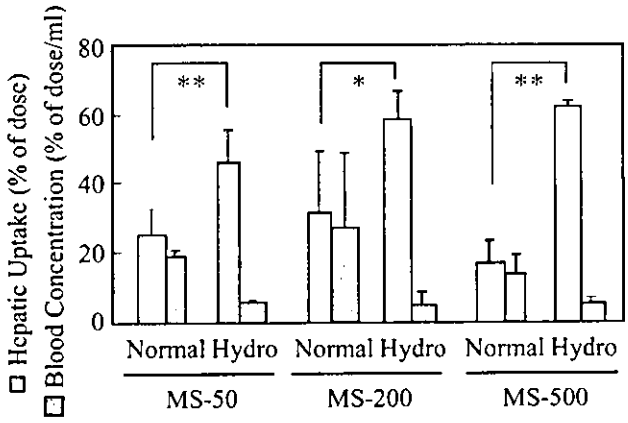

Figure 3. Degree of hepatic uptake and blood concentrations of MS following i.v. injection in $GdCl_3$-treated mice. Mice were treated i.v. with $GdCl_3$ (30 mg/kg) and received MS 24 h later as described in the legend to Figure 1. The results are expressed as the mean ± S.D. of at least three mice. There are significant differences between the procedures; $^*P < 0.05$, $^{**}P < 0.01$

Table 1. Effect of size on the hepatic uptake of MS following the normal and the hydrodynamics-based procedures in $GdCl_3$-treated or untreated mice

	Normal			Hydro		
$GdCl_3$	MS-50	MS-200	MS-500	MS-50	MS-200	MS-500
(−)	100.0 ± 23.0	100.0 ± 21.8	100.0 ± 2.0	95.8 ± 11.3	108.3 ± 8.4	114.6 ± 14.5
(+)	42.7 ± 15.6	45.2 ± 25.0	26.7 ± 11.3	80.6 ± 16.7	82.7 ± 12.6	99.5 ± 4.2

Based on the data shown in Figures 1 and 3, the degree of hepatic uptake of MS following normal injection in $GdCl_3$-untreated mice (defined as the control) was normalized to 100% and the relative degree (±S.D.) of hepatic uptake for the other groups ($GdCl_3$(−) Hydro, $GdCl_3$(+) Normal and $GdCl_3$(+) Hydro) was calculated in terms of the corresponding control.

Localization of MS in hepatocyte suspension following the normal and the hydrodynamics-based procedures

Figures 4 and 5 show the confocal microscopic images of a cellular suspension of hepatocytes isolated from mice which had received an i.v. injection of MS by the normal and the hydrodynamics-based procedures. A large part of the MS-50 injected by the hydrodynamics-based procedure was detected on the surface of the hepatocytes (Figure 4B). Furthermore, some particles of MS-50 appeared in the intracellular compartment following the hydrodynamics-based procedure (Figures 4B–4F). On the other hand, MS-200 and MS-500, for the most part, seemed to be in the extracellular compartment as aggregates (Figures 5B and 5E). While a fraction of MS-200 and MS-500 interacted with the cellular membrane of the hepatocytes, they were not detected intracellularly (Figures 5C and 5F). As expected, almost none of the injected MS was detected in the suspension of hepatocytes following normal injection for all the sizes tested (Figures 4A, 5A, and 5D).

Intrahepatic distribution of MS and transgene-expressing cells in the liver following the hydrodynamics-based procedure

To examine the relative localization of MS and transgene-expressing cells which are likely to be delivered with a sufficient amount of pDNA, either MS-50, MS-200 or MS-500 and pDsRed2-N1 was injected simultaneously into mice by the hydrodynamics-based procedure. As shown in Figure 6, MS was delivered preferentially to the same regions of the liver with pDNA, where transgene-expressing cells were abundant (Figures 6C and 6E). However, in detail, MS-200 and MS-500 were mainly detected extracellularly and, to a lesser extent, intracellularly, and some particles appeared pericellularly in transgene-expressing cells (Figures 6D and 6F). Observation of MS-50 was difficult probably because of the limited resolution and lower signal intensity of single MS-50 particles (Figures 6A and 6B).

Discussion

Nonviral gene delivery, which is regarded as a promising way of *in vivo* gene transfer due to its safety and versatility, has the disadvantage of limited efficacy. The hydrodynamics-based gene delivery of naked pDNA solution gives a significantly high level of transgene expression in the liver and other major organs [1]. Use of the hydrodynamics-based procedure offers a potentially promising method of nonviral gene delivery for therapeutic purposes, even though it requires some acceptable modification such as tissue-selective application. Recently, we demonstrated the mechanism of the procedure as a nonspecific process by which the injected pDNA was delivered directly into the cytosol of hepatocytes through the cellular membrane [5,22]. Thus, the hydrodynamics-based procedure enables pDNA to circumvent one of the most important hurdles, i.e. passage through the cellular membrane and avoidance of endosomal or lysosomal degradation, which conventional carrier systems have to overcome for improved transgene expression [27–30]. When focusing on other hurdles, such as cytosolic stability and nuclear transport of pDNA, we should take a second look at complexation or encapsulation of pDNA to overcome them. In the present study, we have discussed the particle size dependence of the hydrodynamics-based procedure to estimate a suitable size spectrum of solute and to clarify the mechanisms governing the procedure. We note here that polystyrene microspheres (MS), 50, 200 and 500 nm in diameter, were chosen as model particles so that we did not expect encapsulation of pDNA in the MS used in the present study.

We tried to examine the effect of particle size on the hydrodynamics-based procedure by comparing the degree of hepatic uptake of MS with that produced by the normal procedure. The hepatic uptake and blood concentrations of MS were recorded after 10 min since the efficient intracellular gene delivery, which results in a high-level transgene expression, seems to be almost completed within this shorter period in the hydrodynamics-based procedure [22]. In normal mice, MS were effectively taken up by the liver following the normal procedure (Figure 1). The major contributing cells are presumably Kupffer cells, since it is well known that particulates including microspheres are efficiently ingested by liver macrophages, Kupffer cells, via phagocytosis following

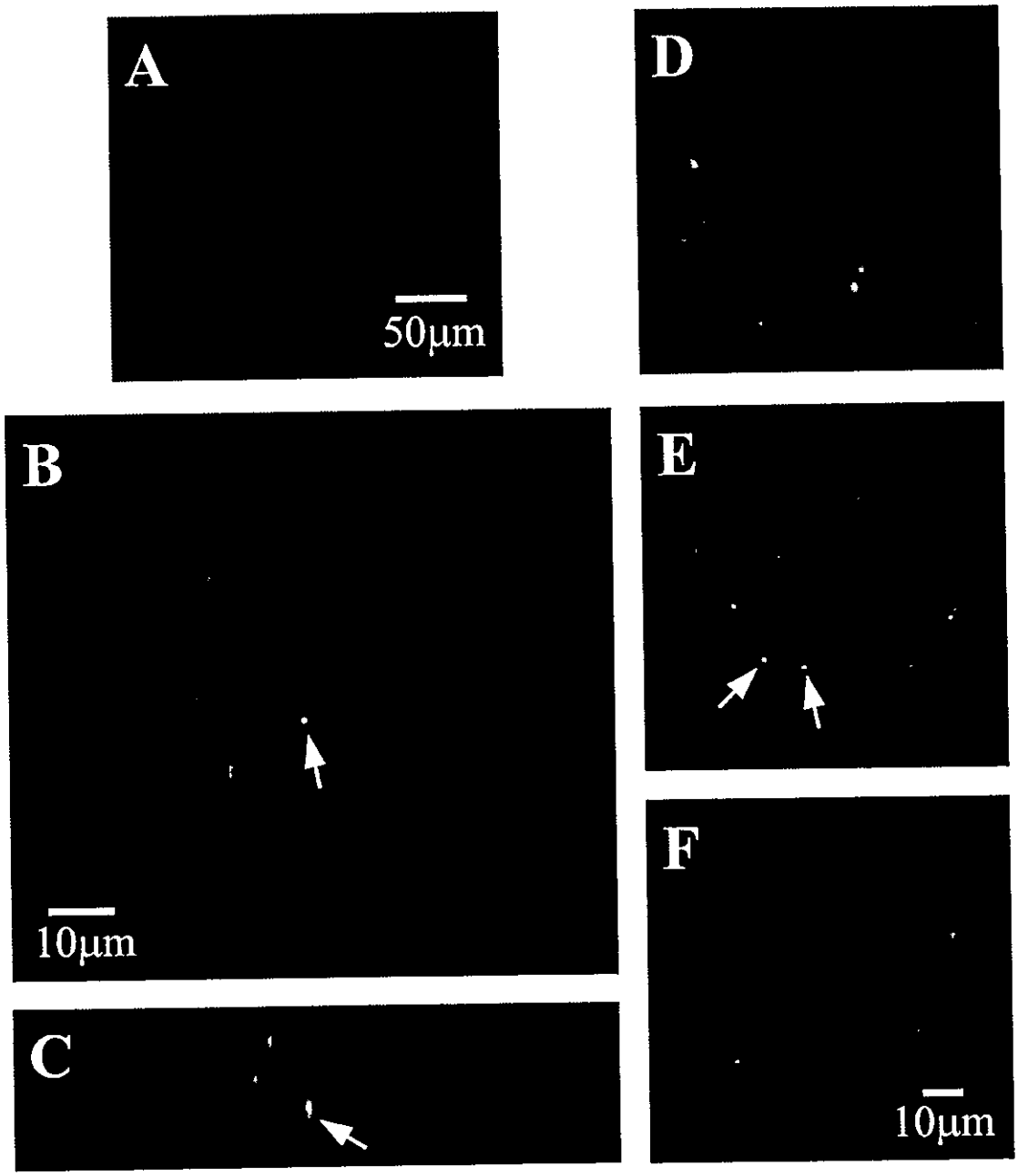

Figure 4. Confocal microscopic images of the cellular suspension of hepatocytes following i.v. injection of MS-50. Ten minutes after an i.v. injection of MS-50 by the normal (A) or the hydrodynamics-based (B–F) procedure, liver parenchymal cells were isolated as described in 'Materials and methods'. Images B and C are X-Y and X-Z scanning sections of the same cells, respectively. Images D, E and F are sequential X-Y scanning sections in this order of the same cells with 2.5 μm intervals between the sections shown. The background signal derived from the cells was strengthened until it was detectable as a weak green color for easier recognition of the cell silhouettes. Arrows indicate intracellular MS detected. The images shown are the typical of those observed in several visual fields. Green: FITC-MS

systemic application [31,32]. In fact, isolation of the liver-constituting cells by centrifugal elutriation has revealed quantitatively that MS-50 and MS-500 were taken up predominantly by Kupffer cells in our previous study [23]. Following the hydrodynamics-based procedure, MS of all sizes tested were taken up by the liver to a similar extent as that of the normal procedure. However, confocal microscopic observation of the liver sections revealed that the intrahepatic distribution of MS was apparently different for the two procedures (Figure 2), suggesting the possibility of a quantitative comparison. Thus, we minimized the phagocytotic effects of Kupffer cells by pre-injection of $GdCl_3$ and discussed the effect of particle size quantitatively by comparing the relative degree of hepatic uptake as described in the legend to Table 1. In $GdCl_3$-treated mice, the degree of hepatic uptake of MS, especially MS-500, was significantly reduced following the normal procedure (Figure 3, Table 1), confirming the larger contribution of Kupffer cells to the hepatic uptake of larger-sized MS. On the other

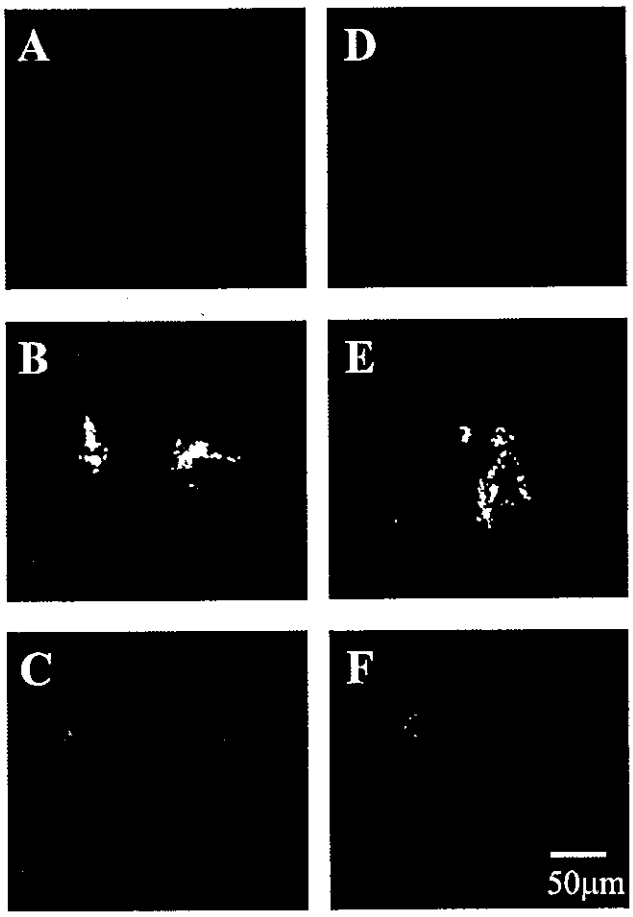

of hepatocytes following i.v. injection of MS-200 and MS-500. Ten minutes after an i.v. injection of MS-200 (A, B, C) or MS-500 (D, E, F) by the normal (A, D) or the hydrodynamics-based (B, C, E, F) procedure, liver parenchymal cells were isolated. The background signal derived from the cells was strengthened until it was detectable as a weak green color for easier recognition of the cell silhouettes. The images shown are typical of those observed in several visual fields. Green: FITC-MS

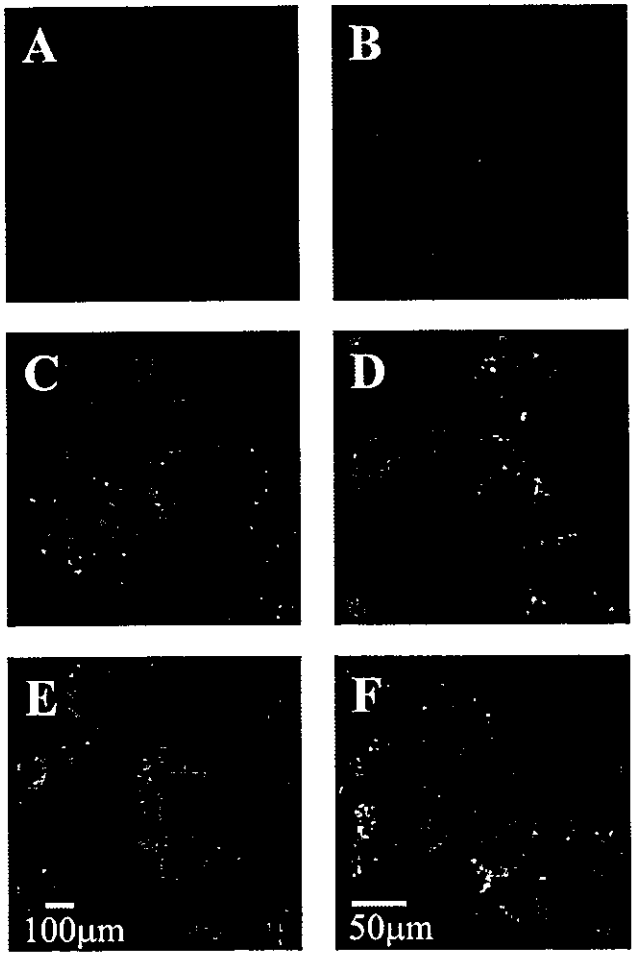

Figure 6. Confocal microscopic images of the liver section following i.v. injections of MS and DsRed-expressing pDNA. Mice received MS-50 (A, B), MS-200 (C, D) or MS-500 (E, F) and pDsRed2-N1 simultaneously by the hydrodynamics-based procedure. At 24 h, the liver was excised and cryosections were made. The images shown are typical of those observed in several visual fields. Green: FITC-MS; red: DsRed

hand, the degree of hepatic uptake of MS was not affected by $GdCl_3$ treatment in the hydrodynamics-based procedure (Figure 3, Table 1), suggesting much less of a contribution by Kupffer cells to the overall hepatic uptake of MS. We also observed a significantly enhanced hepatic delivery by the hydrodynamics-based procedure in $GdCl_3$-treated mice (Figure 3). This phenomenon was most apparent in MS-500 (Table 1), suggesting that the hydrodynamics-based procedure caused extravasation of MS efficiently for larger particles up to 500 nm in diameter. Overall, the hydrodynamics-based delivery resulted in extravasation of MS as in the case of pDNA delivery and promoted interaction of MS with non-Kupffer cells such as hepatocytes and endothelial cells or extracellular matrix. Following extravasation, a fraction of the MS was likely to diffuse back into the sinusoidal space more rapidly in the case of smaller particles.

We next examined the possibility of direct intracellular delivery of MS to hepatocytes and, if it occurred, its particle size dependence. Because hepatocytes are the majority of the liver-constituting-cells and the hydrodynamics-based procedure is supposed to deliver naked pDNA directly into the cytosol of hepatocytes [5,22], we focused on the hepatocytes as the main target of the hydrodynamics-based MS delivery although interaction of MS with other liver cells or components was not excluded. Confocal microscopic studies of freshly isolated hepatocyte suspension revealed that there was a large amount of MS in the extracellular compartment or on the surface of the cellular membrane following the hydrodynamics-based procedure (Figures 4 and 5), confirming the promoted extravasation of MS. Some particles of MS-50 were detected intracellularly, whereas intracellular particles of MS-200 or MS-500 were very rare in our study (Figures 4 and 5). Although, in the present study, we could not estimate quantitatively the extent of hepatocyte internalized or simply cellular-associated MS, these results suggest that MS promoted extravasation in the hydrodynamics-based procedure at all sizes tested and that smaller particles were more susceptible to hydrodynamics-based direct delivery to the hepatocyte

cytosol. The recovery of the isolated hepatocytes was lower in mice undergoing the hydrodynamics-based procedure, probably because the large-volume injection affected the efficacy of collagenase digestion in the liver. Given that the more susceptible regions of the liver to the hydrodynamics-based procedure were more greatly affected regarding the efficacy of collagenase digestion, we can assume that some MS-200 or MS-500 were delivered directly to the hepatocytes while these cells were hardly obtained. It is likely that the direct intracellular delivery of MS is a passive process and not endocytosis since the hepatocytes seem to have less phagocytotic ability of such large particles, suggesting that the mechanism of the efficient hydrodynamics-based pDNA delivery is similar to that of diffusion or a solvent drag-like process.

From our results, the size spectrum applicable to the hydrodynamics-based hepatic delivery is around 50 nm or less in terms of intracellular delivery, although it is apparently required to broaden the size range of MS in order to determine exactly the 'cut-off' size of particles. In the case that delivery to the extracellular spaces of hepatocyte following extravasation is intended or enough, the applicable size spectrum would be in the range 50–500 nm or more, with larger particles being more favorable. Comparing the present results and the fact that a gyration diameter of pDNA measured by a dynamic light scattering spectrophotometer was around 150 nm [33] and the superhelix diameter of pDNA was up to 10 nm [34], the effectively delivered population of naked pDNA which leads to significant transgene expression following the hydrodynamics-based procedure is likely to pass the cellular membrane in a thread-like form or a supercoiled, relatively condensed more compact form. This was supported by the fact that MS were preferentially distributed to the pericellular regions of transgene-expressing cells (Figure 6). The interference in the transgene expression following complexation of pDNA in the hydrodynamics-based procedure [9, Kobayashi *et al.*, unpublished observation] is probably due to the relatively large particle size, although influence of other factors such as net surface charge cannot be excluded, in that most of those complexes were not successfully delivered intracellularly, but trapped in the extracellular compartment.

Although further studies of the particle size dependence of the procedure are required for the construction of more optimal nonviral gene delivery strategies, the hydrodynamics-based gene delivery system has the potential to become an alternative methodology for gene therapy in the immediate future.

Acknowledgement

This work was supported in part by a Grant-in-Aid for Scientific Research from the Ministry of Education, Culture, Sports, Science and Technology, Japan.

References

1. Liu F, Song Y, Liu D. Hydrodynamics-based transfection in animals by systemic administration of plasmid DNA. *Gene Ther* 1999; **6**: 1258–1266.
2. Zhang G, Budker V, Wolff JA. High levels of foreign gene expression in hepatocytes after tail vein injections of naked plasmid DNA. *Hum Gene Ther* 1999; **10**: 1735–1737.
3. Song YK, Liu F, Zhang G, *et al.* Hydrodynamics-based transfection: simple and efficient method for introducing and expressing transgenes in animals by intravenous injection of DNA. *Methods Enzymol* 2002; **346**: 92–105.
4. Maruyama H, Higuchi N, Nishikawa Y, *et al.* High-level expression of naked DNA delivered to rat liver via tail vein injection. *J Gene Med* 2002; **4**: 333–341.
5. Kobayashi N, Kuramoto T, Yamaoka K, *et al.* Hepatic uptake and gene expression mechanisms following intravenous administration of plasmid DNA by conventional and hydrodynamics-based procedures. *J Pharmacol Exp Ther* 2001; **297**: 853–860.
6. Kobayashi N, Kuramoto T, Chen S, *et al.* Therapeutic effect of intravenous interferon gene delivery with naked plasmid DNA in murine metastasis models. *Mol Ther* 2002; **6**: 737–744.
7. Herweijer H, Zhang G, Subbotin VM, *et al.* Time course of gene expression after plasmid DNA gene transfer to the liver. *J Gene Med* 2001; **3**: 280–291.
8. Budker V, Budker T, Zhang G, *et al.* Hypothesis: naked plasmid DNA is taken up by cells in vivo by a receptor-mediated process. *J Gene Med* 2000; **2**: 76–88.
9. Rossmanith W, Chabicovsky M, Herkner K, *et al.* Cellular gene dose and kinetics of gene expression in mouse livers transfected by high-volume tail-vein injection of naked DNA. *DNA Cell Biol* 2002; **21**: 847–853.
10. Lecocq M, Andrianaivo F, Warnier MT, *et al.* Uptake by mouse liver and intracellular fate of plasmid DNA after a rapid tail vein injection of a small or a large volume. *J Gene Med* 2003; **5**: 142–156.
11. Zhang G, Budker V, Williams P, *et al.* Surgical procedures for intravascular delivery of plasmid DNA to organs. *Methods Enzymol* 2002; **346**: 125–133.
12. Zhang G, Vargo D, Budker V, *et al.* Expression of naked plasmid DNA injected into the afferent and efferent vessels of rodent and dog livers. *Hum Gene Ther* 1997; **8**: 1763–1772.
13. Eastman SJ, Baskin KM, Hodges BL, *et al.* Development of catheter-based procedures for transducing the isolated rabbit liver with plasmid DNA. *Hum Gene Ther* 2002; **13**: 2065–2077.
14. Wang Z, Qiu SJ, Ye SL, *et al.* Combined IL-12 and GM-CSF gene therapy for murine hepatocellular carcinoma. *Cancer Gene Ther* 2001; **8**: 751–758.
15. Wu X, He Y, Falo LD Jr, *et al.* Regression of human mammary adenocarcinoma by systemic administration of a recombinant gene encoding the hFlex-TRAIL fusion protein. *Mol Ther* 2001; **3**: 368–374.
16. Yang J, Chen S, Huang L, *et al.* Sustained expression of naked plasmid DNA encoding hepatocyte growth factor in mice promotes liver and overall body growth. *Hepatology* 2001; **33**: 848–859.
17. Loser P, Jennings GS, Strauss M, *et al.* Reactivation of the previously silenced cytomegalovirus major immediate-early promoter in the mouse liver: involvement of NFkappaB. *J Virol* 1998; **72**: 180–190.
18. Mazda O. Improvement of nonviral gene therapy by Epstein-Barr virus (EBV)-based plasmid vectors. *Curr Gene Ther* 2002; **2**: 379–392.
19. Yew NS, Zhao H, Przybylska M, *et al.* CpG-depleted plasmid DNA vectors with enhanced safety and long-term gene expression in vivo. *Mol Ther* 2002; **5**: 731–738.
20. Godbey WT, Wu KK, Mikos AG. Tracking the intracellular path of poly(ethylenimine)/DNA complexes for gene delivery. *Proc Natl Acad Sci U S A* 1999; **96**: 5177–5181.
21. Wang J, Zhang PC, Mao HQ, *et al.* Enhanced gene expression in mouse muscle by sustained release of plasmid DNA using PPE-EA as a carrier. *Gene Ther* 2002; **9**: 1254–1261.
22. Kobayashi N, Nishikawa M, Hirata, *et al.* Hydrodynamics–based procedure involves transient hyperpermeability in the hepatic cellular membrane: implication of a nonspecific process in efficient intracellular gene delivery. *J Gene Med*; in press.

23. Ogawara K, Yoshida M, Higaki K, *et al.* Hepatic uptake of polystyrene microspheres in rats: effect of particle size on intrahepatic distribution. *J Control Release* 1999; **59**: 15–22.
24. Ogawara K, Furumoto K, Takakura Y, *et al.* Surface hydrophobicity of particles is not necessarily the most important determinant in their in vivo disposition after intravenous administration in rats. *J Control Release* 2001; **77**: 191–198.
25. Hardonk MJ, Dijkhuis FW, Hulstaert CE, *et al.* Heterogeneity of rat liver and spleen macrophages in gadolinium chloride-induced elimination and repopulation. *J Leukoc Biol* 1992; **52**: 296–302.
26. Nishikawa M, Takemura S, Takakura Y, *et al.* Targeted delivery of plasmid DNA to hepatocytes in vivo: optimization of the pharmacokinetics of plasmid DNA/galactosylated poly(L-lysine) complexes by controlling their physicochemical properties. *J Pharmacol Exp Ther* 1998; **287**: 408–415.
27. Nishikawa M, Huang L. Nonviral vectors in the new millennium: delivery barriers in gene transfer. *Hum Gene Ther* 2001; **12**: 861–870.
28. Davis ME. Non-viral gene delivery systems. *Curr Opin Biotechnol* 2002; **13**: 128–131.
29. Niidome T, Huang L. Gene therapy progress and prospects: nonviral vectors. *Gene Ther* 2002; **9**: 1647–1652.
30. Pouton CW, Seymour LW. Key issues in non-viral gene delivery. *Adv Drug Deliv Rev* 1998; **34**: 3–19.
31. Moghimi SM, Davis SS. Innovations in avoiding particle clearance from blood by Kupffer cells: cause for reflection. *Crit Rev Ther Drug Carrier Syst* 1994; **11**: 31–59.
32. Illum L, Davis SS. The organ uptake of intravenously administered colloidal particles can be altered using a non-ionic surfactant (Poloxamer 338). *FEBS Lett* 1984; **167**: 79–82.
33. Nishikawa M, Yamauchi M, Morimoto K, *et al.* Hepatocyte-targeted in vivo gene expression by intravenous injection of plasmid DNA complexed with synthetic multi-functional gene delivery system. *Gene Ther* 2000; **7**: 548–555.
34. Hammermann M, Brun N, Klenin KV, *et al.* Salt-dependent DNA superhelix diameter studied by small angle neutron scattering measurements and Monte Carlo simulations. *Biophys J* 1998; **75**: 3057–3063.

Gene Therapy (2004) 11, 901–908

www.nature.com/gt

RESEARCH ARTICLE

Restoration of dystrophin expression in mdx mice by intravascular injection of naked DNA containing full-length dystrophin cDNA

KW Liang[1], M Nishikawa[1], F Liu[1], B Sun[1], Q Ye[2] and L Huang[1]
[1]Center for Pharmacogenetics, School of Pharmacy, University of Pittsburgh, Pittsburgh, PA, USA; and [2]Department of Biological Sciences, Carnegie Mellon University, Pittsburgh, PA, USA

Duchenne muscular dystrophy (DMD) is a lethal, X-linked, recessive disease caused by a defect in the dystrophin gene. No effective therapy is available. Dystrophin gene transfer to skeletal muscle has been proposed as a treatment for DMD. However, successful treatment for DMD requires restoration of dystrophin in the affected muscle fibers to at least 20% of the normal level. Current gene transfer methods such as intramuscular injection of viral vector or naked DNA can only transfect a small area of muscle, and therefore is of little clinical utility. We have developed a semisystemic method for gene transfer into skeletal muscle of mdx mice, an animal model for DMD. Naked DNA was injected through the tail artery or vein of mice, in which the aorta and the vena cava were clamped at the location just below the kidneys. The DNA solution was thus forced into the blood vessels of both legs. Luciferase gene expression was detected in all muscle groups in both legs. The effects of injection speed, injection volume, and ischemia time on gene expression were also optimized. LacZ staining was used to check the spread of gene expression in muscle. Although the percentage of transfected fibers was modest (~ 10%), β-galactosidase was found in all muscle groups of both legs. Finally, plasmid DNA encoding full-length dystrophin gene was injected into mdx mice and widespread restoration of dystrophin protein was observed in all muscles of both hind limbs. In conclusion, these results demonstrate that the semisystemic delivery of naked DNA is a potential approach towards the long-term goal of gene therapy for DMD.
Gene Therapy (2004) **11**, 901–908. doi:10.1038/sj.gt.3302239
Published online 26 February 2004

Keywords: *nonviral vector; naked DNA; muscle; Duchenne muscular dystrophy*

Introduction

Duchenne muscular dystrophy (DMD) is a common X-linked progressive muscular disorder that occurs at the frequency of one in 3500 male births. Most of the affected males die of respiratory or heart failure around the third decade of life.[1–3] This severe muscle disorder is caused by the absence of a muscle cytoskeleton protein, dystrophin. Restoration of dystrophin protein expression by gene therapy is apparently an important method that may offer a cure for this disease. However, the widespread loss of the dystrophin protein in all muscles of an affected individual represents a major challenge for the development of an effective gene therapy treatment. For this reason, the development of a systemic delivery system, which can ideally deliver dystrophin gene into all muscles, is imperative to the success of gene therapy for DMD.

Gene transfer of dystrophin gene to skeletal muscle has mainly been carried out by intramuscular injection of naked DNA[4] or viral vector.[5–9] Unfortunately, it is unlikely that direct intramuscular injection of naked DNA is a clinically viable method of delivering gene into DMD patients. First of all, the level of gene expression is too low to have any sufficient significance. More importantly, the muscle fibers expressing the transgene product is very spatially limited; gene expression only occurs in a few square centimeters near the injection site.

Neutral polymers, such as polyvinyl pyrrolidone, have been used to enhance gene expression in muscle; however, there is no significant improvement in the area of gene expression.[10] Intravascular delivery of naked DNA to muscle is apparently an attractive approach for overcoming this problem, because it would permit DNA to reach all muscle fibers, thereby leading to more widespread therapeutic gene expression.

Recently, Budker *et al*[11] developed a semisystemic method that could deliver plasmid DNA into a whole leg of a rat They injected DNA solution through the femoral artery of rats while all blood vessels to and from the leg were occluded. Gene expression was detected in all muscle groups of the leg. This method represents a significant advance towards the development of gene therapy for DMD. More importantly, Zhang *et al*[12] has demonstrated the applicability of this method in primate. However, the applicability of this method to restore dystrophin protein on DMD animal models, such as mouse or dog, remains unknown.

In this study, we report a semisystemic delivery method that can efficiently transfect all muscles in both

Correspondence: L Huang, Center for Pharmacogenetics, School of Pharmacy, University of Pittsburgh, Pittsburgh, PA 15213, USA
Received 19 May 2003; accepted 23 December 2003; published online 26 February 2004

hind limbs of mice. We demonstrate that it is possible to achieve widespread restoration of dystrophin protein in all hind-limb muscles of *mdx* mice by intravascular injection of naked DNA encoding the dystrophin gene. We also investigate factors that limit the naked DNA delivery through intravascular injection. These results have important implications with regard to the development of gene therapy for DMD.

Results

Injection route

To examine any difference in gene expression in the muscle after DNA injection through the tail artery or tail vein, 100 μg of DNA in 2 ml phosphate-buffered saline (PBS) solution was injected through either the tail artery or tail vein, while the aorta and vena cava were clamped (Figure 1). At 2 days after injection, muscle was collected and luciferase gene expression in all muscle groups was measured. As shown in Figure 2, a relatively high level of gene expression could be detected in all muscle groups in both cases. In addition, the level of gene expression was about 10-fold greater in mice receiving DNA through the tail artery than in those injected through the tail vein. Furthermore, the levels of gene expression in one leg by the tail vein injection could be dramatically enhanced when the blood flow through the other leg was blocked (data not shown). The tail vein injection, technically speaking, is easier to perform than the artery injection.

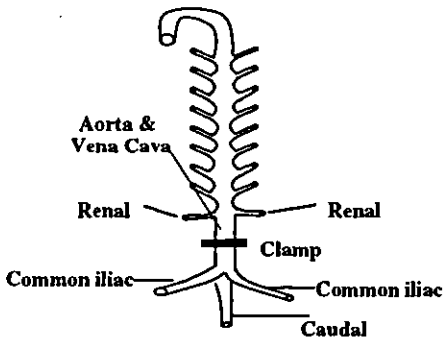

Figure 1 Schematic illustration of tail artery and tail vein injection of DNA solution. DNA PBS solution (2 ml) was injected through the tail artery, while the aorta and vena cava were clamped as indicated.

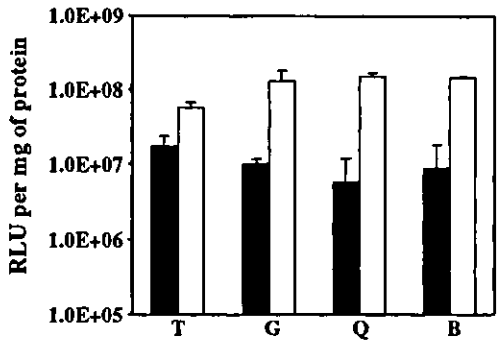

Figure 2 Effect of intravenous and intra-artery injection on gene expression in muscles. DNA (100 μg) in 2 ml PBS solution were injected either through the tail vein (close bar) or the tail artery (open bar), while the blood flow in the aorta and vena cava was occluded. Gene expression in biceps and semitendinous (B), gastrocnemius (G), quadriceps (Q) and tibialis (T) were examined 48 h after injection. Data represent mean ± s.d. (n = 5).

Injection speed, volume, and ischemia time

To optimize the condition of injection for gene transfer, we examine the effects of injection speed, injection volume, and ischemia time on gene expression in muscles. To study the effect of injection speed, 2 ml of DNA solution containing 100 μg of luciferase plasmid were injected through the tail artery of mice in 5 or 20 s. Luciferase gene expression in mouse legs was examined 2 days later (Figure 3a). Gene expression in those mice

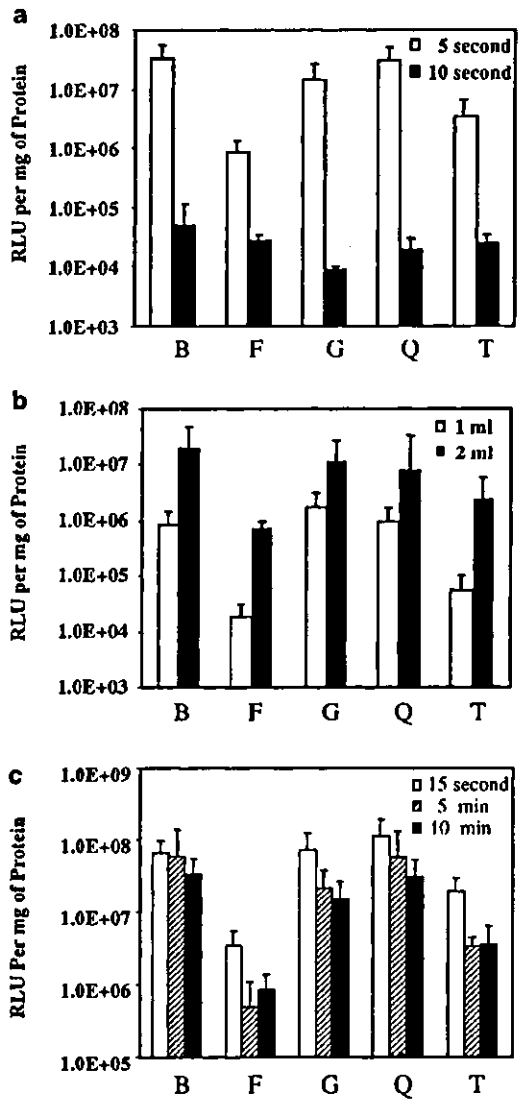

Figure 3 Effect of injection speed, volume and ischemia time on gene expression in mouse legs. DNA (100 μg) in 2 ml PBS solution was injected through the tail artery in 5 or 20 s (a) or DNA in 1 or 2 ml PBS was injected in 5 s (b), while the aorta and vena cava were clamped for 15 s, 5 or 10 min, respectively (c). Gene expression in biceps and semitendinous (B), foot (F), gastrocnemius (G), quadriceps (Q) and tibialis (T) were examined 48 h after injection. Data represent mean ± s.d. (n = 5).

where the DNA solution were injected within 5 s were about a thousand times higher than that in the mice where the DNA solution were injected in 20 s. This result indicates that hydrodynamic pressure induced by injection within a short time period is important for muscle gene transfer.

In another series of experiment, the effect of injection volume was examined. A measure of 1, 2 or 3 ml of DNA solution was injected into mice within 5 s and the luciferase gene expression was examined 2 days later (Figure 3b). Injection of 1 ml DNA solution resulted in gene expressions more than 10-fold lower than those injected with 2 ml DNA solution. Further increase in injection volume did not result in significant increase in gene expression (result not shown for 3 ml injection). This result together with the result of injection speed indicates that increased hydrodynamic pressure is critical for naked DNA delivery to the muscle.

To examine whether high pressure should be maintained after the injection to achieve high levels of gene expression, the blood flow was blocked for different periods of time. Figure 3c shows that there was no significant difference in gene expression in muscles whether the blood flow was blocked for 15 s, 5, or 10 min after DNA was injected. This result indicates that maintaining a high pressure is probably not a critical factor once the DNA is delivered to the muscle tissue.

Effect of histamine on gene expression

As the extravasation of plasmid DNA might be limited by the presence of endothelium, we tested whether histamine, which increases the endothelium permeability, could increase the gene expression in the muscle (Figure 4). In mice preinjected with histamine, gene expressions in all different muscle groups were more than 10-fold higher than in mice preinjected with PBS. This result indicates that the endothelium is one of the major barriers for naked DNA delivery to the muscle.

DNA dose–response

Three doses of luciferase DNA were tested for gene expression in muscles. Mice were injected with 25, 100, or 200 μg luciferase DNA in 2 ml PBS solution in 5 s and muscles were collected 2 days after of injection. The results are shown in Figure 5. Gene expression in all muscle groups increased with increasing amount of DNA injected. Even with the injection of 200 μg of DNA, no saturation has observed. It is known that in intramuscular injection, the uptake of DNA normally saturates at 100 μg of DNA.[13] The reason for this discrepancy could be due to the fact that intra-artery injection can deliver plasmid to many more muscle fibers, therefore the cell surface available for DNA uptake is much greater than the case for intramuscular injection. In addition, our method of occlusion does not guarantee that the DNA solution only flows to the muscle; some could be delivered to the abdominal organs.

Time course of DNA expression

Intramuscular injection of plasmid DNA results in a relatively long period of gene expression.[14] To examine whether this is the same with intra-artery injection, luciferase expression was measured at various time points after intra-artery injection of 100 μg of DNA in 2 ml of saline solution. The results are shown in Figure 6. The gene expression reached its peak between 1 and 2 weeks. After 2 weeks, gene expression started to decline. At 1 month, gene expression in muscles was about 50% of the peak level. This result suggests that the duration of gene expression after intra-artery injection is comparable to that of the intramuscular injection.

Study of LacZ gene expression in muscle

To examine the percentage of muscle fibers transfected by intra-artery injection of plasmid, 400 μg of plasmid containing the *lacZ* gene in 2 ml PBS solution were injected. Figure 7 shows that large numbers of myofibers expressing the *lacZ* gene product could be observed 7 days after the injection of plasmid DNA. Unlike gene expression using intramuscular injection, *lacZ* gene expression after intra-artery administration was much more widely spread. This is evident in all muscle groups (data not shown). However, the percentage of muscle

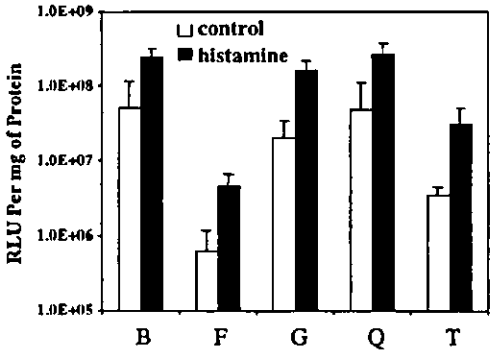

Figure 4 Effect of histamine on gene expression in mouse legs. DNA (2 ml) in PBS solution were injected through the tail artery, while the aorta and vena cava were clamped. At 5 min prior to the DNA injection, 1 ml PBS (control) or 1 ml histamine (histamine) in PBS were injected through the tail artery. Gene expressions were examined 48 h after injection. Data represent mean ± s.d. of luciferase activity in biceps and semitendinous (B), foot (F), gastrocnemius (G), quadriceps (Q) and tibialis (T) (n = 5).

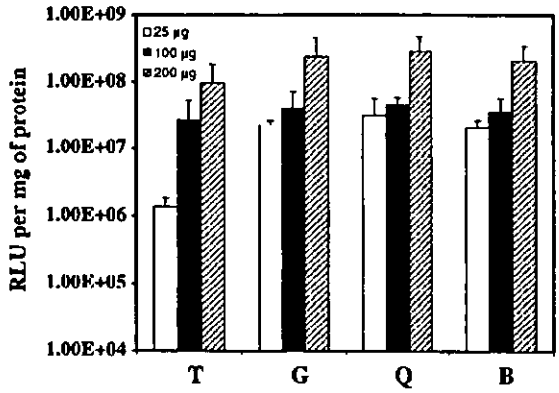

Figure 5 Dose–response of luciferase gene expression in different groups of mouse muscles. Biceps and semitendinous (B), gastrocnemius (G), quadriceps (Q) and tibialis (T) of mice were examined for luciferase gene expression 2 days after the mice were injected with different amounts of luciferase plasmid in 2 ml PBS solution through the tail artery. Data represent mean ± s.d. (n = 4).

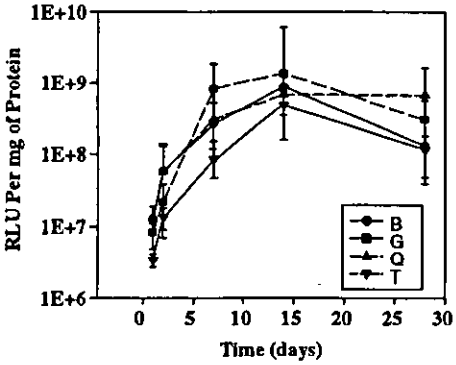

Figure 6 Time course of gene expression in mouse legs after intra-artery injection. DNA (100 μg) in 2 ml PBS solution were injected through the tail artery, while the aorta and vena cava were clamped. Gene expression in biceps and semitendinous (b), gastrocnemius (G), quadriceps (Q) and tibialis (T) were examined at 1, 2, 7, 14 and 28 days after the injection. Data represent mean±s.d. (n=4).

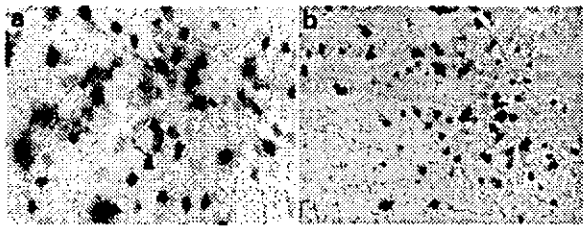

Figure 7 LacZ gene expression in the muscle after intraartery injection. LacZ activity staining was carried out on the quadriceps muscles 7 days after intra-artery injection of 400 μg LacZ DNA in PBS. Magnification ×200 (a); ×100 (b).

fibers transfected was modest; about 10% of muscle fibers were transfected as defined by LacZ expression.

Plasmid distribution in muscle tissue

As the percentage of muscle fibers transfected was modest by intra-artery injection of plasmid, we wondered whether plasmid DNA had reached all muscle cells by this method of delivery. To answer the question, plasmid DNA was labeled with rhodamine-labeled peptide nucleic acid (PNA) so that the plasmid DNA still maintained a supercoiled conformation after labeling.[15] We examined the plasmid distribution at 5 and 30 min after intra-artery injection. As shown in Figure 8, at 5 min after injection, almost all muscle fibers were surrounded by red-colored plasmid DNA. At 30 min, plasmid DNA started to be seen inside some of the cells, but the majority of DNA still remained outside the cells. This result indicates that plasmid DNA can overcome the endothelial barrier by injection through the tail artery. However, the muscle cell membrane seemed to become the main barrier for the uptake of naked DNA delivered intravascularly.

Effect of intra-artery injection on muscle integrity

Large volume of injection solution is required to increase the hydrodynamic pressure inside the blood vessel so that plasmid DNA can be forced to pass through the endothelial wall. One major concern of this method of delivery is whether the injection will cause severe damage to muscle cells. To address this issue, we

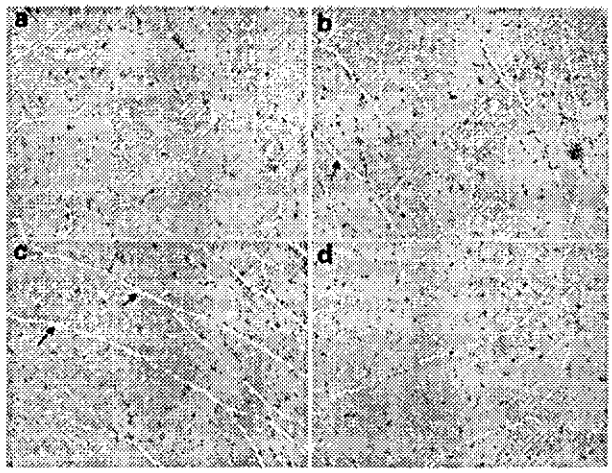

Figure 8 Naked DNA distribution in muscles after intra-artery injection. Rhodamine-labeled DNA (100 μg) in 2 ml PBS solution were injected through the tail artery. Muscles were collected at 5 min (a, c) and 30 min (b, d). Photomicrographs were taken at ×200 (a, b) and ×100 magnifications (c, d).

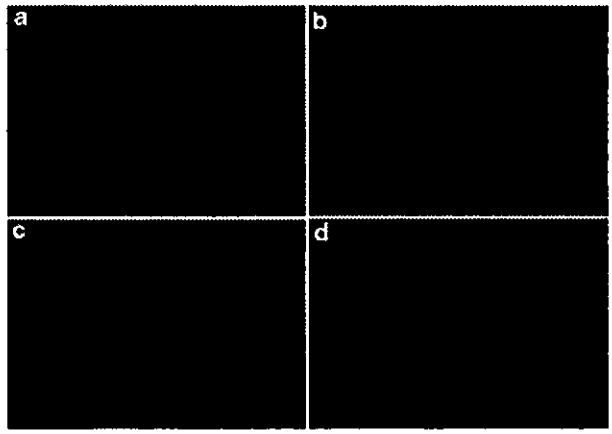

Figure 9 Histology of mouse quadriceps. Quadriceps were collected from untreated mouse (a) or mice 2 days (b, c) or 7 days (d) after injection with 100 μg luciferase plasmid in 2 ml PBS solution through the tail artery. Magnification ×200. Arrows indicate the widening of space between interstitial space.

examined the morphology of muscle fibers by hematoxylin and eosin (H&E) staining after intra-artery injection of 2 ml DNA solution. Muscles were collected and examined 2 and 7 days after injection. As shown in Figure 9, muscles showed slight widening of the interstitial endomysial space 2 days after injection. However, there was no evidence of muscle damage at this time point. By 7 days after injection, muscles displayed a normal histological appearance (Figure 9). No inflammation, nor lymphocyte or leukocyte infiltration, was evident in both time points, indicating that intra-artery injection of plasmid DNA does not induce adverse immunological reaction in the muscle.

Restoration of full-length dystrophin protein

The efficacy of expression of full-length dystrophin cDNA by intra-artery (Figure 10a) or tail vein injection (Figure 10b) was examined 7 days after injection of

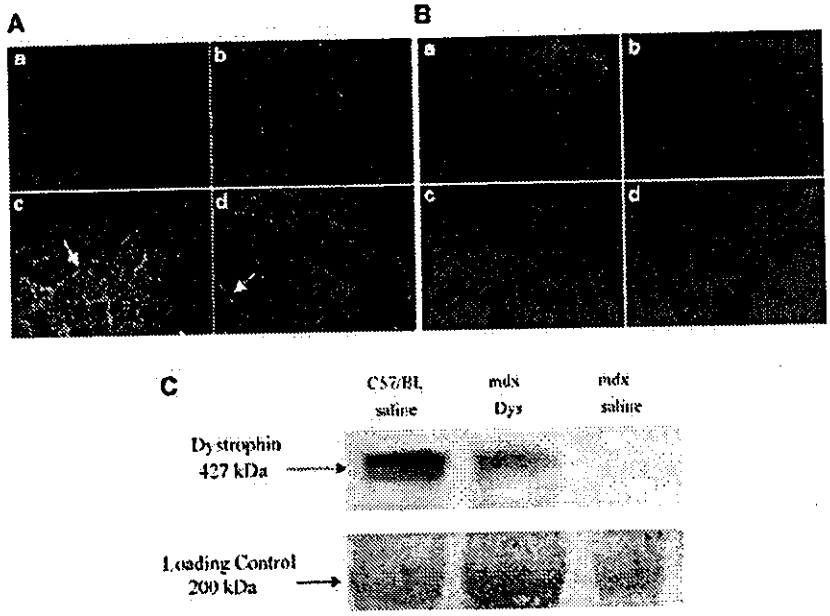

Figure 10 Immunofluorescence localization of dystrophin and Western blot for dystrophin assay. pFDPC (500 μg) containing the full-length dystrophin cDNA were injected through the aorta (Figure 10A). Quadriceps (c) and gastrocnemius (d) of the treated mdx mice were collected 7 days after the injection. Controls are cross-sections of quadriceps from untreated mdx (a) and C57/BL10 (b) mice. Green fluorescence indicates dystrophin staining and blue fluorescence indicates nuclei stained with DAPI. Arrows indicate possible staining of the vasculature. The same amount of dystrophin cDNA was injected through the tail vein flowing clamping the aorta and vena cava and occluding the blood flow through one of legs (Figure 10B,C). The dystrophin staining was carried out by using a polyclonal antidystrophin antibody 6–10. Controls were the sections of quadriceps from C57/BL10 (a) and untreated mdx (b). Quadriceps (c) and gastrocnemius (d) of the treated mdx mice were collected 7 days after the injection. Magnification × 100. Top panel in Figure 10c: Western blotting of total protein extracted from the mice quadraceps treated with saline or dystrophin gene Lower panel: Bands of myosin (200 kDa) on the post-transfer Commossie gel serving as loading control.

Table 1 Percentage of myofibers expressing dystrophin in different muscle groups*

Muscle groups	*% of dystrophin-positive fibers*
Quadriceps	52±25
Biceps and semitendinous	45±29
Gastrocnemius	38±28
Tibialis	27±30

Muscles were examined 7 days after intra-artery injection of full-length dystrophin plasmid. The high variation is due to the uneven distribution of dystrophin gene.

500 μg of plasmid DNA containing full-length murine dystrophin cDNA into the *mdx* or wild-type C57 mice (Figure 10). Immunofluorescence staining of normal skeletal muscle in C57 mice revealed dystrophin as a continuous staining along the plasma membrane of every muscle fiber. In untreated *mdx* mice, this pattern of staining was not observed. On the other hand, the dystrophin-positive fibers were clearly observed in *mdx* mice injected with full-length dystrophin plasmid. Even though the level of dystrophin expressed were lower than that of C57 mice, more than 30% of muscle fibers in all muscle groups are dystrophin positive (Table 1). In treated *mdx* mice, some vasculatures (arrows in Figure 10a) were also stained due to nonspecificity of the method used. The data for intravenous injection (Figure 10b) is very similar to that of the intra-artery injection (Figure 10a). The quantitative analysis of the bands of Western blot in Figure 10c by NIH Imager 1.6 showed about 31% of dystrophin expression, compared to the C57/BL mice, when mdx mice were transferred with dystrophin gene.

Discussion

The pathological severeness of DMD has prompted extensive research on developing gene therapy methods for the treatment of this chronic but deadly disease. Different methods including myoblast transplantation[16] and gene transfer have been explored. Among the gene transfer methods, viral vectors such as herpes simplex virus (HSV),[17] adenovirus[18,19,7] and adeno-associated virus[20,8,9] or nonviral vectors including HVJ liposome[21] and naked DNA have been tested. Although viral vectors can achieve high degrees of gene transfer efficiency, their use for the delivery of dystrophin has encountered many problems. For example, although HSV and adenoviral vectors can deliver the full-length dystrophin gene, they both suffer from strong immune response in the host and loss of infectivity when muscle fibers are mature.[22] Adeno-associated viral vectors, on the other hand, are capable of efficiently infecting both young and mature muscle fibers, but their small packaging limit makes it impossible to deliver full-length dystrophin gene. Compared to viral vectors, the use of naked DNA to treat DMD has certain advantages. First, naked DNA appears to have no significant side effects when delivered to muscle. Although there are some reports with regard to inflammatory responses arising from the CpG motifs on the plasmid DNA,[23,24] intra-artery injection of naked

DNA does not seem to cause any significant inflammation as demonstrated in our study (Figure 9). This may be because of the absence of cationic carrier, which normally enhance the inflammatory response.[25] Furthermore, skeletal muscle seems to internalize naked DNA more efficiently than other types of tissue.[26]

Our study demonstrates that it is possible to achieve widespread gene expression in skeletal muscles by intravascular injection of naked DNA. Gene expression was detected in all muscle groups in either one or both hind limbs of mice (Figures 2–5 and 10, Table 1). There are apparently two major barriers for intravascular delivery of naked DNA to skeletal muscles. The first barrier is the endothelium wall, which apparently limits the extravasation of naked DNA to reach the muscle tissue. It was reported that the endothelium in muscle is different from the endothelium in liver or spleen. The latter is noncontinuous and fenestrated, containing many large pores. The former is of continuous and nonfenestrated type.[27] Despite its small size, naked DNA apparently cannot pass through the endothelium freely. In fact, the endothelium barrier is not only a barrier for naked DNA but also a barrier for viral vectors such as adenoviral and adeno-associated viral vectors as well.[28,29] For gene therapy to be successful for systemic muscular disorders such as DMD, overcoming the endothelium barrier becomes the first prerequisite. Increasing the hydrodynamic pressure by injecting a large volume of DNA solution within a short time period seems to be an effective method to overcome this barrier. This method has been applied for both naked DNA- and viral vector-mediated gene transfer to muscles.[11,28,29] A relatively large volume of solution in the vasculature may expand the endothelium and stretch the pores on the endothelium. Second, the elevated hydrodynamic pressure in the vasculature may force the DNA solution to pass through the endothelium and disperse it in the muscle tissue. Our results also showed a significant difference between intravenous injection and intra-artery injection. This significant difference may be simply due to the fact that arteries are less distensible than veins and so the plasmid solution is transmitted directly to the capillaries, where the hydrostatic pressure forces the solution into the interstitial space. In contrast, delivery via the venous system would lead to pooling of the plasmid solution in the veins as they can expand to accommodate very large volumes. In addition, major veins have valves that act to prevent blood flowing back towards the capillaries and these may have a barrier effect when venous delivery to the hind limbs is attempted. Other methods have also been used to enhance the extravasation of DNA. For example, Budker *et al*[11] have combined vasodilator and collagenase, which can digest the basal membrane of the endothelium, to increase the permeability of the endothelium and they observed further increase of gene expression. In our study, we have used histamine to increase the permeability of the endothelium. In histamine-treated mice, gene expression was enhanced about 10-fold in all muscle groups of the mouse legs. The application of histamine to increase the extravasation of adenoviral vector has also been tested and similar level of enhancement in gene expression was observed.[29] The combination of large volume injection with some agents that can increase the endothelium permeability seems to be an effective method to overcome the endothelium barrier.

The second barrier for gene delivery to skeletal muscle appears to be the cellular uptake of naked DNA. Using fluorescence-labeled plasmid DNA, we clearly demonstrate that our method can deliver plasmid DNA to almost all muscle fibers in the tissue (Figure 8). However, only a relatively small percentage of muscle fibers showed gene expression when LacZ was used as a reporter gene. Therefore, muscle fibers seem to resist naked DNA uptake. This barrier appears to be the major barrier for gene delivery to skeletal muscle. Overcoming this barrier will have significant implication for gene therapy for DMD.

Compared to intramuscular injection, in which only a few percent of muscle fibers are been transfected, our method represents a significant advancement. Although in our LacZ study, the percentage of muscle fibers expressing LacZ is still low, the gene was expressed in all the muscle groups in mouse legs. Furthermore, it was reported that LacZ staining normally underestimates the gene expression about three-fold.[30] Indeed, our immunostaining with dystrophin gene expression revealed a much wider area of gene expression (Figure 10 and Table 1). However, it is not clear whether muscle function can be restored at this expression level. Function studies are required to assess the effect. Furthermore, data shown in Figure 10 seem to indicate that dystrophin was also expressed in the vasculature cells of the treated mouse. This could be due to the fact that the dystrophin gene used in this study was not controlled by a muscle-specific promoter. With the development of more efficient DNA vectors such as the ones with a targeting ligand attached,[31] and with the use of a muscle-specific gene expression system, specific gene expression may be further increased.

In summary, the results of our study demonstrates the possibility of systemic delivery of naked DNA and achieve widespread expression of dystrophin gene in multiple skeletal muscles in *mdx* mice. However, the practical application of this method to treat DMD is still limited by the relatively low efficiency of DNA uptake by muscle cells and relatively short period of transgene expression. In addition, injecting large volume of solution locally may be applicable to human, as demonstrated by Zhang *et al*,[12] in monkeys. However, the application of this method to the diaphragm would be problematic. Different delivery method for the naked DNA to the diaphragm has recently been reported by this lab.[32] It is possible to treat DMD by treating different organs separately. However, before this can happen, problems such as transfection efficiency and short-term expression have to be overcome.

Materials and methods

Plasmids

pCMV-Luc plasmid containing firefly luciferase cDNA driven by CMV immediate-early promoter was constructed by introducing the luciferase cDNA into pNGVL3 plasmid (National Gene Vector Laboratory, University of Michigan, MI, USA). pCMVLacZ plasmid was obtained from Invitrogen (Palo Alto, CA, USA). pFDPC plasmid containing full-length dystrophin cDNA

under the control of CMV promoter was constructed by digesting pSRαDMD (a gift from Dr Paula Clemens) with *Not*I and ligating to the *Not*I site of pcDNA 3 (Invitrogen, Palo Alto, CA, USA). For plasmid distribution study, pWIZ-Lux plasmid obtained from Gene Therapy System (GTS, San Diago, CA, USA) was labeled with rhodamine-labeled PNA according to a previous report.[15] All plasmids were amplified in *Escherichia coli* and purified by Qiagen Giga plasmid preparation kit (Qiagen, Valencia, CA, USA).

Animal procedures

All experiments were performed using CD-1 mice (4–6 weeks old) or X-linked muscular dystrophy (mdx) mice (4–6 weeks old). Prior to any surgical procedure, the animals were anesthetized by intraperitoneal injection of 2,2,2-tribromoethanol (500 mg/kg). For plasmid injection, the tail artery or tail vein was cannulated with a 25 G butterfly needle connected to a polyethylene tubing (Harvard Apparatus, Holliston, MA, USA). The needle was subsequently fixed to the tail with instant adhesive (Loctite 404, Applied Industrial Technology, Pittsburgh, PA, USA). The abdomen was then opened to expose the aorta and the vena cava. Prior to injection, a microvascular clamp (Harvard Apparatus, Holliston, MA, USA) was placed on the aorta and vena cava at the location just below the kidneys (Figure 1) so that the DNA solution can pass through the common iliac artery and reach the leg muscles after injection from the tail artery or tail vein. In a typical experiment, 2 ml of PBS solution containing 100 μg of luciferase plasmid or 400 μg of β-galactosidase plasmid was injected in 5 s. Alternatively, DNA solution was injected to mice through the tail vein following clamping the aorta, vena cava and occlusion of the blood flow through one of the legs using modified artery forceps. The clamps were removed 15 s after injection and mice were allowed to recover from the effect of anesthesia. To examine the effect of histamine, 1 ml of PBS with or without histamine (10 mM) was first injected, and 5 min later, 2 ml of luciferase plasmid solution was then injected.

For the administration of dystrophin plasmid, the aorta of *mdx* mice was cannulated with a microcannula (Harvard Apparatus, Holliston, MA, USA), 1.5 ml of 10 mM histamine solution in PBS containing 500 μg of the full-length dystrophin plasmid was injected in 5 s. After injection, the incision on aorta was closed with suture and mice were allowed to recover from the effect of anesthesia.

β-Galactosidase expression analysis

At 1 week after the intravascular injection of pCMVLacZ, mice were killed by cervical dislocation. All muscle groups were harvested and flash-frozen in isopentane cooled in liquid nitrogen. Serial cross-sections (12 μm) were placed onto glass slides (Super-frost plus; Fisher Scientific, Pittsburgh, PA, USA) and kept at –80°C. X-gal staining was carried out using X-galactosidase staining kit (Invitrogen, Palo Alto, CA, USA) according to the manufacture's procedure. Briefly, muscle sections were fixed in 1% glutaldehyde for 10 min and then rinsed with PBS. Sections were then stained overnight for β-galactosidase activity by incubation at 37°C with 5-bromo-4-chloro-3-indolyl-β-D-galactopyranoside (X-gal, 1 mg/ml), 1 mM $MgCl_2$, 5 mM potassium ferrocyanide, and 5 mM potassium ferricyanide in PBS. After washing in PBS, the slides were counterstained in alcoholic eosin and then dehydrated and mounted. Photographs were taken with a Nikon TE-300 fluorescence microscope. To quantitate the percentage of LacZ-positive fibers, the number of positive cells and the total number of cells were counted from 15 photographs covering different areas of muscle section.

Luciferase gene expression analysis

For luciferase assay, the entire muscle groups were collected from each mouse leg 2 days after injection, except for the time-course study. The muscles were homogenized in lysis buffer (1% Triton X-100, 2 mM EDTA, 0.1 M Tris, pH 7.8) using a tissue tearer (Biospec Products, Bartlesville, OK, USA). The homogenates were centrifuged at 14 000 *g* for 10 min at 4°C and 10 μl of the supernatant was analyzed for luciferase activity using an LB 953 luminometer (Berthod). The results were expressed as relative light units per mg of tissue protein. Protein assay was carried out with the Coomassie plus reagent (Pierce, Rockford, IL, USA).

Plasmid distribution and histological examination of the muscle damage

PBS (2 ml) solution containing 100 μg of luciferase plasmid labeled with rhodamine-PNA was injected through the tail artery as described above. At 5 and 30 min after injection, the quadriceps were collected, flash-frozen and sectioned. The slides were examined and photographed using a Nikon T-300 fluorescence microscope. For the muscle damage study, 2 ml of PBS solution containing luciferase plasmid was injected as above. Quadriceps were collected at 2 and 7 days after injection, sectioned and stained with H&E.

Immunofluorescence detection of dystrophin gene expression

Serial crosscryosections (6 μm) were collected. Immunostaining of dystrophin was performed with the Mouse-on-Mouse Kit (Vector Laboratories) according to the manufacturer's protocol without fixing the muscle sections. Primary monoclonal antibody against the C-terminus of dystrophin (NCL-Dys2; 1:20 dilution) was purchased from NovoCastra Laboratories (Burlingame, CA, USA). Muscle cell nuclei were counterstained with a mounting medium containing 4', 6'-diamidino-2-phenylindole (DAPI) (Vector Laboratories). For quantitation of dystrophin-positive fibers, the number of dystrophin-positive cells and the total number of cells were counted from 15 photographs covering different areas of muscle section. For intravenously injected animals, the sections were preincubated for 1 h at room temperature with 10% horse serum in PBS (pH 7.4) and then incubated overnight with affinity purified rabbit polyclonal anti-dystrophin antibody 6–10 (a gift from EP Hoffman).[33,34] After four rinses in 10% horse serum/PBS, the sections were incubated with Alexa Fluor 568 goat anti-rabbit antibody (Molecular Probes, 1:200 dilution) for 1 h. As controls, the muscle sections from C57BL/10 and untreated *mdx* mice were similarly processed. The sections were examined and photographed with a Nikon TE-300 fluorescence microscope.

Dystrophin assay by Western blot

Methods. Mice quadriceps were sectioned and extracted at TEE buffer that contains 20 mM Tris pH 8.0, 1 mM EDTA, 1 mM EGTA and then mixed with same volume of 10% SDS and incubate in ice for 30 min. Protein concentration was determined using BCA protein assay kit (Biorad). The samples were then subjected to electrophoresis of 7.5% SDS-PAGE gel, transferred to nitrocellulose membrane. Dystrophin expression was then detected using a high-affinity antidystrophin antibody anti 6–10, a generous gift from Dr LM Kunkel (Children's hospital and Harvard Medical School, Boston, MA, USA), and visualized with anti-rabbit secondary antibody linked to horseradish peroxidase and chemiluminescence (Amersham).

Acknowledgements

This work was supported in part by Muscular Dystrophy Association grant and NIH grant PO1 AR45925 (L. Huang) and grant from the Uehara memeriol Foundation (M. Nishikawa). We thank Dr Paula Clemens for providing the dystrophin plasmid and *mdx* mice. Kenneth W Liang and Makiya Nishikawa were postdoctoral fellows of Duchenne Muscular Dystrophy Research Center, University of Pittsburgh.

References

1 Hoffman EP, Brown Jr RH, Kunkel LM. Dystrophin: the protein product of the Duchenne muscular dystrophy locus. *Cell* 1987; **51**: 919–928.
2 Zubrzycka-Gaarn EE *et al*. The Duchenne muscular dystrophy gene product is localized in sarcolemma of human skeletal muscle. *Nature* 1988; **333**: 466–469.
3 Campbell KP, Kahl SD. Association of dystrophin and an integral membrane glycoprotein. *Nature* 1989; **338**: 259–262.
4 Acsadi G *et al*. Human dystrophin expression in mdx mice after intramuscular injection of DNA constructs [see comments]. *Nature* 1991; **352**: 815–818.
5 Deconinck N *et al*. Functional protection of dystrophic mouse (mdx) muscles after adenovirus-mediated transfer of a dystrophin minigene. *Proc Natl Acad Sci USA* 1996; **93**: 3570–3574.
6 Yang L *et al*. Adenovirus-mediated dystrophin minigene transfer improves muscle strength in adult dystrophic (MDX) mice. *Gene Therapy* 1998; **5**: 369–379.
7 Gilbert R *et al*. Prolonged dystrophin expression and functional correction of mdx mouse muscle following gene transfer with a helper-dependent (gutted) adenovirus-encoding murine dystrophin. *Hum Mol Genet* 2003; **12**: 1287–1299.
8 Harper SQ *et al*. Modular flexibility of dystrophin: implications for gene therapy of Duchenne muscular dystrophy. *Nat Med* 2002; **8**: 253–261.
9 Watchko J *et al*. Adeno-associated virus vector-mediated minidystrophin gene therapy improves dystrophic muscle contractile function in mdx mice. *Hum Gene Ther* 2002; **13**: 1451–1460.
10 Mumper RJ *et al*. Protective interactive noncondensing (PINC) polymers for enhanced plasmid distribution and expression in rat skeletal muscle. *J Control Rel* 1998; **52**: 191–203.
11 Budker V *et al*. The efficient expression of intravascularly delivered DNA in rat muscle. *Gene Therapy* 1998; **5**: 272–276.
12 Zhang G *et al*. Efficient expression of naked DNA delivered intraarterially to limb muscles of nonhuman primates. *Hum Gene Ther* 2001; **12**: 427–438.
13 Levy MY *et al*. Characterization of plasmid DNA transfer into mouse skeletal muscle: evaluation of uptake mechanism, expression and secretion of gene products into blood. *Gene Therapy* 1996; **3**: 201–211.
14 Wolff JA *et al*. Long-term persistence of plasmid DNA and foreign gene expression in mouse muscle. *Hum Mol Genet* 1992; **1**: 363–369.
15 Zelphati O *et al*. Gene chemistry: functionally and conformationally intact fluorescent plasmid DNA. *Hum Gene Ther* 1999; **10**: 15–24.
16 Karpati G *et al*. Dystrophin is expressed in mdx skeletal muscle fibers after normal myoblast implantation. *Am J Pathol* 1989; **135**: 27–32.
17 Akkaraju GR *et al*. Herpes simplex virus vector-mediated dystrophin gene transfer and expression in MDX mouse skeletal muscle. *J Gene Med* 1999; **1**: 280–289.
18 Acsadi G *et al*. Dystrophin expression in muscles of mdx mice after adenovirus-mediated *in vivo* gene transfer. *Hum Gene Ther* 1996; **7**: 129–140.
19 Jani A *et al*. Generation, validation, and large scale production of adenoviral recombinants with large size inserts such as a 63 kb human dystrophin cDNA. *J Virol Methods* 1997; **64**: 111–124.
20 Wang B, Li J, Xiao X. Adeno-associated virus vector carrying human minidystrophin genes effectively ameliorates muscular dystrophy in mdx mouse model. *Proc Natl Acad Sci USA* 2000; **97**: 13714–13719.
21 Yanagihara I *et al*. Expression of full-length human dystrophin cDNA in mdx mouse muscle by HVJ-liposome injection. *Gene Therapy* 1996; **3**: 549–553.
22 Feero WG *et al*. Viral gene delivery to skeletal muscle: insights on maturation-dependent loss of fiber infectivity for adenovirus and herpes simplex type 1 viral vectors. *Hum Gene Ther* 1997; **8**: 371–380.
23 Krieg AM *et al*. CpG motifs in bacterial DNA trigger direct B-cell activation. *Nature* 1995; **374**: 546–549.
24 McMahon JM *et al*. Inflammatory responses following direct injection of plasmid DNA into skeletal muscle. *Gene Therapy* 1998; **5**: 1283–1290.
25 Whitmore M, Li S, Huang L. LPD lipopolyplex initiates a potent cytokine response and inhibits tumor growth. *Gene Therapy* 1999; **6**: 1867–1875.
26 Davis HL *et al*. Plasmid DNA is superior to viral vectors for direct gene transfer into adult mouse skeletal muscle. *Hum Gene Ther* 1993; **4**: 733–740.
27 Taylor A, Granger D. The cardiovascular system: microcirculation. In: Renkin E, Michel CC, Geiger SR (eds). *Handbook of Physiology*, Am. Physiol. Soc.: Bethesda, MD 1984: 467–520.
28 Cho WK *et al*. Modulation of Starling forces and muscle fiber maturity permits adenovirus-mediated gene transfer to adult dystrophic (mdx) mice by the intravascular route. *Hum Gene Ther* 2000; **11**: 701–714.
29 Greelish JP *et al*. Stable restoration of the sarcoglycan complex in dystrophic muscle perfused with histamine and a recombinant adeno-associated viral vector. *Nat Med* 1999; **5**: 439–443.
30 Couffinhal T *et al*. Histochemical staining following LacZ gene transfer underestimates transfection efficiency. *Hum Gene Ther* 1997; **8**: 929–934.
31 Liang KW, Hoffman EP, Huang L. Targeted delivery of plasmid DNA to myogenic cells via transferrin-conjugated peptide nucleic acid. *Mol Ther* 2000; **1**: 236–243.
32 Liu F *et al*. Transfer of full-length Dmd to the diaphragm muscle of Dmd(mdx/mdx) mice through systemic administration of plasmid DNA. *Mol Ther* 2001; **4**: 45–51.
33 Koenig M, Kunkel LM. Detailed analysis of the repeated domain of dystrophin reveals 4 potential hinge regions that may confer flexibility. *J Biol Chem* 1990; **265**: 4560–4566.
34 Hoffman EP *et al*. Somatic reversion/suppression of the mouse *mdx* phenotype *in vivo*. *J Neurol Sci* 1990; **99**: 9–25.

Immunology 2004 **111** 282–290

doi: 10.1111/j.1365-2567.2004.01814.x

Restricted cytokine production from mouse peritoneal macrophages in culture in spite of extensive uptake of plasmid DNA

KEI YASUDA, HIROKI KAWANO, IKUKO YAMANE, YOSHIYUKI OGAWA, TAKAHARU YOSHINAGA, MAKIYA NISHIKAWA & YOSHINOBU TAKAKURA *Department of Biopharmaceutics and Drug Metabolism, Graduate School of Pharmaceutical Sciences, Kyoto University, Sakyo-ku, Kyoto, Japan*

SUMMARY

The production of inflammatory cytokines from macrophages (Mϕ), upon stimulation with plasmid DNA (pDNA) containing CpG motifs, is a critical process for DNA-based therapies such as DNA vaccination and gene therapy. We compared Mϕ activation, following stimulation with naked pDNA, based on the production of cytokines from cell lines (RAW264.7 and J774A1) and peritoneal Mϕs in primary culture. The Mϕ cell lines RAW264.7 and J774A1 produced a significant amount of tumour necrosis factor-α (TNF-α) upon stimulation with naked pDNA and this response required endosomal acidification. On the other hand, peritoneal Mϕs (both resident and elicited) in primary culture did not secrete TNF-α or interleukin-6, although they contain the mRNA of toll-like receptor-9 (TLR-9) and are able to respond to CpG oligodeoxynucleotides. This unresponsiveness was not a result of impaired cellular uptake of pDNA because the primary cultured Mϕs showed a higher uptake of pDNA than the RAW264.7 and J774A1 cell lines. These findings have important implications for Mϕ activation by naked pDNA as it has been generally assumed that pDNA that contains CpG motifs is a potent agent for inducing inflammatory cytokines *in vivo*, based on evidence from *in vitro* studies using Mϕ cell lines.

INTRODUCTION

Bacterial DNA and plasmid DNA (pDNA) contain a relatively high frequency of unmethylated CpG dinucleotides (CpG motifs), which are suppressed and methylated in vertebrate DNA. The immune system has evolved a defence mechanism based on the recognition of these CpG motifs.[1,2] For example, bacterial DNA and CpG oligodeoxynucleotides (ODN) can activate cells of the innate immune system, such as macrophages (Mϕs) and dendritic cells (DCs), to secrete pro-inflammatory cytokines, including tumour necrosis factor-α (TNF-α), interleukin (IL)-1, IL-6 and IL-12.[3–7] This phenomenon appears to be advantageous as far as DNA vaccination is concerned[8] because it is crucial in the subsequent development of T-helper 1 (Th1)-biased T-cell lineages in response to CpG DNA.[9–11] On the other hand, recent reports have demonstrated that these inflammatory cytokines inhibit transgene expression with pDNA.[12,13] Therefore, cytokine production from Mϕs upon stimulation with pDNA containing CpG motifs is a critical process in the application of DNA-based therapies, such as DNA vaccination and gene therapy.

Recently it was reported that Toll-like receptor-9 (TLR-9), expressed in Mϕs and DCs, recognizes the CpG motifs.[14,15] As a first cytosolic event, the adaptor molecule MyD88 is recruited to the receptor complex, followed by engagement of IL-1 receptor-associated kinase (IRAK) and the adapter molecule, TRAF6.[16] Oligomerization of TRAF6 leads to the activation of downstream kinases, such as the stress kinase JNK1/2 and the IκB kinase (IKK) complex.[17] This, in turn, results in activation of transcription factors such as AP-1 and nuclear factor (NF)-κB. Proof of these phenomena has been obtained using synthetic phosphorothioate CpG ODN (S-ODN), small single-stranded DNA. It is generally assumed that the same mechanism would be involved in cellular activation by pDNA because its backbone contains similar immunostimulatory sequences. In fact, a variety of studies have demonstrated that CpG motifs are required to stimulate immune responses following DNA vaccination.

Received 28 October 2003; revised 4 December 2003; accepted 9 December 2003.

Abbreviations: DC, dendritic cell; FBS, fetal bovine serum; IL, interleukin; LPS, lipopolysaccharide; Mϕ, macrophage; ODN, oligodeoxynucleotides; pDNA, plasmid DNA; TCA, trichloroacetic acid; TLR, toll-like receptor; TNF-α, tumour necrosis factor-α.

Correspondence: Yoshinobu Takakura, Department of Biopharmaceutics and Drug Metabolism, Graduate School of Pharmaceutical Sciences, Kyoto University, 46-29, Yoshidashimoadachi-cho, Sakyo-ku, Kyoto 606-8501, Japan. E-mail: takakura@pharm.kyoto-u.ac.jp